

# Many-body parametric resonances in the driven sine-Gordon model

Izabella Lovas,<sup>1,2,3</sup> Roberta Citro,<sup>4,5</sup> Eugene Demler,<sup>6,7</sup>  
Thierry Giamarchi,<sup>8</sup> Michael Knap,<sup>1,2</sup> and Edmond Orignac<sup>9</sup>

<sup>1</sup>*Department of Physics, Technical University of Munich, 85748 Garching, Germany*

<sup>2</sup>*Munich Center for Quantum Science and Technology (MCQST), Schellingstr. 4, 80799 München, Germany*

<sup>3</sup>*Kavli Institute for Theoretical Physics, University of California, Santa Barbara, CA 93106, USA*

<sup>4</sup>*Dipartimento di Fisica "E.R. Caianiello", Università degli Studi di Salerno and CNR-SPIN  
c/o University of Salerno, Via Giovanni Paolo II, 132, I-84084 Fisciano (Sa), Italy*

<sup>5</sup>*INFN, Sezione di Napoli, Gruppo collegato di Salerno, I-84084 Fisciano (SA), Italy*

<sup>6</sup>*Department of Physics, Harvard University, Cambridge, MA 02138, USA*

<sup>7</sup>*Institute for Theoretical Physics, ETH Zurich, 8093 Zurich, Switzerland*

<sup>8</sup>*DQMP, University of Geneva, 24 Quai Ernest-Ansermet, CH-1211 Geneva, Switzerland*

<sup>9</sup>*ENSL, CNRS, Laboratoire de physique, F-69342 Lyon, France*

(Dated: April 14, 2022)

We study a quantum many-body variant of the parametric oscillator, by investigating the driven sine-Gordon model with a modulated tunnel coupling via a semi-classical Truncated Wigner Approximation (TWA). We first analyze the parametric resonant regime for driving protocols that retain our model gapped, and compare the TWA to a Time-Dependent Variational Principle (TDVP). We then turn to a drive which closes the gap, resulting in an enhanced energy absorption. While the TDVP approach breaks down in this regime, we can apply TWA to explore the dynamics of the mode-resolved energy density, and the higher-order correlations between modes in the prethermal heating regime. For weak driving amplitude, we find an exponentially fast energy absorption in the main resonant mode, while the heating of all remaining modes is almost perfectly suppressed on short time scales. At later times, the highly excited main resonance provides effective resonant driving terms for its higher harmonics through the non-linearities in the Hamiltonian, and gives rise to an exponentially fast heating in these particular modes. We capture the strong correlations induced by these resonant processes by evaluating higher order connected correlation functions. Our results can be experimentally probed in ultracold atomic settings, with parallel one-dimensional quasi-condensates in the presence of a modulated tunnel coupling.

## I. INTRODUCTION

In recent years, the advances in ultracold atomic experiments paved the way to study novel quantum many-body states, as well as non-equilibrium phenomena in unprecedented detail [1–3]. These systems provide an ideal platform to prepare interesting interacting many-body states in a controlled way, and allow for probing their dynamics. One of the paradigmatic many-body models investigated in these settings is the sine-Gordon model [4], realized by coupling two parallel quasi-one-dimensional bosonic condensates in a double well potential [5–12]. The experimental realization of this model enabled the demonstration and characterization of non-Gaussian higher order correlations in the system, revealed the presence of topological soliton excitations through the full distribution of the spatially resolved relative phase between the two condensates [6], and also lead to the observation of prethermalization in the non-equilibrium dynamics of the model [6, 7].

One of the interesting, only partially explored aspects of the out-of-equilibrium dynamics of the sine-Gordon model is the nature of transient states in the presence of a periodic Floquet drive. Previous works on this model have focused either on regimes of small modulations, within the reach of linear response [13, 14] or on the limit of fast modulations, revealing a sharp crossover in the

heating rate, separating regimes of strongly suppressed heating from regions with efficient energy absorption [15]. The less explored regime of slow driving frequencies offers many open questions regarding the quantum counterpart of well established classical phenomena, such as parametric resonance or amplification due to a resonant driving force [16–22], as well as about the universal aspects of the heating [14, 18, 23]. In particular, the non-linear coupling between modes redistributes the energy absorbed by the resonant mode, and can transiently stop the heating at a finite energy density, while at late times, when many-body scattering is taken into account, the system is expected to heat to an infinite temperature state [18]. This Floquet prethermalization effect has been demonstrated by investigating the total energy of various slowly driven many-body systems [17, 18], however, the detailed mode-resolved energy absorption, shedding light on the dominant non-linearities in quantum systems, is much less explored. The driven sine-Gordon model provides an ideal, experimentally accessible platform to address these unresolved questions.

In this work, we investigate the mode-resolved energy absorption of the slowly driven sine-Gordon model in the presence of a modulated tunnel coupling, constituting a quantum many-body analogue of a parametric oscillator. This system is experimentally accessible in various cold atomic platforms, in particular, by coupling two parallel, quasi-one-dimensional bosonic condensates through

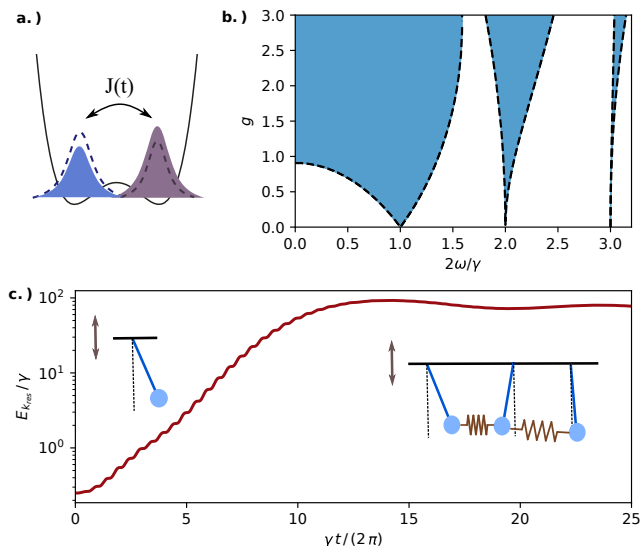


Figure 1. Parametric resonance in quasi-one-dimensional condensates in a modulated double well potential. **a.)** Experimental realization of the driven sine-Gordon model with coupled condensates in an oscillating trap. **b.)** Phase diagram of a classical parametric oscillator, revealing lobes of unstable heating regions (blue) as a function of frequency ratio  $2\omega/\gamma$  and driving amplitude  $g$ , with natural frequency  $\omega$  and driving frequency  $\gamma$ . **c.)** Exponentially fast energy absorption in the resonant mode  $k_{\text{res}}$  of the sine-Gordon model. Heating at short times is analogous to a single resonant parametric oscillator, whereas the saturation on longer time scales reflects a collection of oscillators, coupled through the interaction term.

a modulated double well potential [6, 24–26], see Fig. 1a. Alternatively, the modulated tunnel coupling can also be realized by introducing a Raman coupling between two internal states of the cold atoms [27–29]. In contrast to previous studies focusing on the limit of fast modulations [15], we consider a slow driving frequency tuned to parametric resonance with one of the low energy modes of the static Hamiltonian. Hence, this system realizes a quantum many-body counterpart of the parametric oscillator, with non-linear coupling terms between modes.

The phase diagram of a single classical parametric oscillator is shown in Fig. 1b, displaying lobes of unstable heating regions as a function of the frequency  $\gamma$  and amplitude  $g$  of the drive [30, 31]. In particular, a resonant drive leads to an exponentially fast energy absorption for arbitrarily weak driving amplitude. We demonstrate an analogous exponential heating for the resonant mode in the full quantum many-body system in Fig. 1c, evaluated with the semi-classical Truncated Wigner Approximation [32] (TWA), allowing for calculating the time evolution for various driving protocols. We also compare these results to another approach, the Time-Dependent Variational principle (TDVP), whenever applicable. The TWA results show that the early stages of the dynamics can be well understood in terms of a single parametric oscillator. However, at longer time scales the non-linear

coupling between modes cuts off the fast energy absorption, and leads to saturation, similarly to the prethermal behavior found in the driven  $O(N)$  model [17, 18]. Moreover, we find that the highly excited resonant mode can serve as an effective resonant drive for the higher harmonics through the non-linear coupling terms, leading to an efficient heating in these modes. This heating process occurs in separate stages. First, the main resonance is occupied, while the heating of other modes remains strongly suppressed. Second, the highly excited main resonance serves as a drive for its higher harmonics, with strength increasing in time as the resonant mode becomes even stronger populated. We show that these efficient coupling terms between the main resonance and its higher harmonics give rise to a characteristic pattern in higher-order correlation functions.

The paper is organized as follows. We outline the derivation of the sine-Gordon model from the Hamiltonian of two coupled one-dimensional quasi-condensates in Sec. II A, and discuss the effect of a parametric drive within a linear approximation in Sec. II B. We first focus on driving protocols that keep the gap of the spectrum open in in Sec. III, allowing us to compare TWA to the TDVP. We sketch the derivation of the TDVP in Sec. III A, and present the results of both approaches in Sec. III B. We turn to driving protocols which close the gap in Sec. IV, resulting in an enhanced energy absorption. In this regime we have to rely on TWA to follow the time evolution of the mode resolved energy absorption of the system. We concentrate on the heating of the main resonance and its higher harmonics in Sec. IV A, and find deviations from the behavior of uncoupled oscillators. We construct a simple toy model to explain the main features our findings in Sec. IV B, and test it by examining the correlations between modes in Sec. IV C. We summarize our results and comment on the experimental realization in Sec. V. Technical details are discussed in the appendices.

## II. DRIVEN SINE-GORDON MODEL

### A. Sine-Gordon description of coupled one-dimensional quasi-condensates

The dynamics of two Josephson-coupled one-dimensional interacting quasi-condensates can be well approximated by the sine-Gordon model. To this end, we consider two quasi-one-dimensional bosonic gases, described by the Hamiltonian [33, 34]

$$H_0 = \sum_{j=1,2} \int dx \left\{ \frac{1}{2m} \partial_x \psi_j^\dagger(x) \partial_x \psi_j(x) + \frac{g}{2} \psi_j^\dagger(x) \psi_j^\dagger(x) \psi_j(x) \psi_j(x) \right\}, \quad (1)$$

that are coupled by a time dependent Josephson tunneling term,

$$H_J = -J(t) \int dx \left[ \psi_1^\dagger(x) \psi_2(x) + \psi_2^\dagger(x) \psi_1(x) \right]. \quad (2)$$

Here  $\psi_1(x), \psi_2(x)$  stand for the bosonic fields of the two quasi-condensates,  $g$  denotes the effective one dimensional interaction, depending sensitively on the shape of the transverse trapping potential,  $J(t)$  is the modulated tunneling amplitude, and we have set  $\hbar = 1$ . For simplicity, we focus on homogeneous condensates, moreover, we use periodic boundary conditions in the numerical simulations. We will discuss the effects of open boundary conditions where relevant.

It is convenient to rewrite the field operators in terms of the conjugate phase  $\varphi_j(x)$  and density  $\rho_j(x)$  fluctuations

$$\psi_j(x) = \sqrt{\rho_j(x)} e^{i\varphi_j(x)}. \quad (3)$$

Substituting Eq. (3) into the Hamiltonian leads to a hydrodynamical description of the condensates [35, 36]. To leading order in the density and phase fluctuations, the relative phase  $\varphi = \varphi_2 - \varphi_1$  and density  $\delta\rho = \rho_2 - \rho_1$  decouples from the total phase and density,  $\varphi_1 + \varphi_2$  and  $\rho_1 + \rho_2$ . The dynamics of the relative coordinates is governed by the sine-Gordon Hamiltonian, see appendix A and Refs. 5 and 37,

$$H = \frac{c}{2} \int dx \left\{ \frac{\pi}{K} \delta\rho^2 + \frac{K}{\pi} (\partial_x \varphi)^2 \right\} - 2J(t) \rho_0 \int dx \cos \varphi, \quad (4)$$

with  $c$  denoting the sound velocity,  $K$  the Luttinger parameter, and  $\rho_0$  the average density of the homogeneous gas. Here, the Luttinger parameter  $K$  characterizes the strength of interactions, with  $K \rightarrow \infty$  and  $K = 1$  representing the non-interacting limit and the limit of hard-core bosons, respectively. In the absence of tunnel-coupling,  $J(t) \equiv 0$ , Hamiltonian (4) reduces to a Luttinger-liquid with a linear spectrum,

$$\varepsilon_k = ck. \quad (5)$$

By contrast, a non-zero static tunnel-coupling,  $J(t) \equiv J_0$ , introduces a gap to the dispersion relation. For large  $J_0$ , where the phase is pinned around  $\varphi(x) \sim 0$ , the expansion of the cosine function gives the approximation

$$\varepsilon_k^{\text{gap}} \approx \sqrt{c^2 k^2 + \Delta_0^2}, \quad (6)$$

with

$$\Delta_0 = \sqrt{\frac{2\pi J_0 \rho_0 c}{K}}. \quad (7)$$

In the numerical calculations, we focus on the lattice-regularized version of Eq. (4), obtained by introducing

a lattice spacing  $a$ , and particle number operators  $n_j = a \delta\rho(ja)$ ,

$$H_{\text{Lat}} = \frac{c}{2} \sum_{j=1}^{N_s} \left( \frac{\pi}{Ka} n_j^2 + \frac{K}{\pi a} (\varphi_j - \varphi_{j-1})^2 \right) - 2J(t) \rho_0 a \sum_{j=1}^{N_s} \cos \varphi_j. \quad (8)$$

Here  $N_s$  denotes the number of lattice sites, and the particle number and phase operators satisfy the canonical commutation relations

$$[n_i, \varphi_j] = -i\delta_{i,j}.$$

The model (8) is known as the quantum Frenkel-Kontorova[38, 39] chain.

Our main tool used for exploring the dynamics of Hamiltonian (8) is the semi-classical truncated Wigner approximation. This approach allows us to calculate time-dependent expectation values and correlations by sampling the classical phase and particle number variables  $\{\varphi_j, n_j\}$  randomly at  $t = 0$ , according to the Wigner distribution of the initial state, and by calculating the time evolution from the mean-field equations of motion [32]. The validity of this approximation for studying quantum quenches in the sine-Gordon model has been studied in various works [32, 37, 40], establishing TWA as a reliable approach up to intermediate times and comparatively weak interactions, for the regime that is the main focus of the paper.

## B. Parametric drive

We consider the sine-Gordon Hamiltonian (8) in the presence of a periodically modulated tunnel coupling,

$$J(t) = J_0 + J_1 \sin(\gamma t). \quad (9)$$

First we comment on driving protocols where  $J(t) > 0$  at all times, i.e. the instantaneous spectrum remains gapped throughout the time evolution, in Sec. III. In this case we can compare the semi-classical TWA to another widely used approximation, the TDVP. Then in Sec. IV we turn to the main focus of the paper, the case with zero static component,  $J_0 = 0$ . Here, the gap closes and the potential energy  $\sim J(t) \cos \varphi$  changes sign in each half period of the drive, giving rise to an enhanced energy absorption. For that case the TDVP breaks down because the gap closes, however, the TWA is still well suited for studying the mode resolved energy absorption. Note that for  $J_0 = 0$  the static part of the Hamiltonian is a purely quadratic Luttinger-liquid, displaying the spectrum (5), and allowing to resolve the dynamics according to the modes of the static Hamiltonian.

In order to study the quantum many-body counterpart of the classical parametric oscillator, we tune the driving

frequency  $\gamma$  to parametric resonance with one of the low energy modes,

$$\gamma = 2\varepsilon_{k_{\text{res}}} \quad (10)$$

with  $k_{\text{res}} = 2\pi n_{\text{res}}/N_s$ ,  $n_{\text{res}} \in \mathbb{Z}$ . To gain more insight into the dynamics, it is convenient to consider the classical equation of motion for the phase field  $\varphi_j$ ,

$$\partial_t^2 \varphi_j = \frac{c^2}{a^2} (\varphi_{j+1} + \varphi_{j-1} - 2\varphi_j) - \frac{2\pi J(t)\rho_0 c}{K} \sin \varphi_j, \quad (11)$$

and apply the linear expansion  $\sin \varphi_j \approx \varphi_j$ . For simplicity, here we set the static tunnel coupling to zero,  $J_0 = 0$ . By performing a Fourier transformation and introducing the dimensionless time  $\tau = \varepsilon_{k_{\text{res}}} t$  and wave number  $\tilde{k} = k/k_{\text{res}}$ , we obtain the following Mathieu equation [30, 41]

$$\left( \partial_\tau^2 + \tilde{k}^2 - 2\tilde{g} \sin(2\tau) \right) \varphi_{\tilde{k}} = 0. \quad (12)$$

Here, we have introduced the dimensionless driving amplitude

$$\tilde{g} = -\frac{4\pi J_1 \rho_0 c}{\gamma^2 K}. \quad (13)$$

The Mathieu equation (12) has been obtained by neglecting the coupling between modes, therefore describes a collection of independent parametric oscillators. It can be solved exactly in terms of Mathieu functions [30, 41], and the solution takes the form  $\varphi_{\tilde{k}} = e^{i\nu(\tilde{k}, \tilde{g})P(\tau)}$ , where the function  $P(\tau)$  is periodic in  $\tau$ . The energy absorption of mode  $\tilde{k}$  is thus determined by the so-called Mathieu exponent  $\nu(\tilde{k}, \tilde{g})$ . A negative imaginary part  $\text{Im}\nu(\tilde{k}, \tilde{g}) < 0$  gives rise to exponentially fast heating, whereas a real  $\nu(\tilde{k}, \tilde{g})$  corresponds to a stable, oscillating solution. Inspecting the imaginary part of  $\nu(\tilde{k}, \tilde{g})$  as a function of  $\tilde{k}$  and  $\tilde{g}$  gives rise to the single-oscillator phase diagram, Fig. 1b, with the substitution  $\omega \leftrightarrow \tilde{k}$ .

The Mathieu exponent  $\nu(\tilde{k}, \tilde{g})$  depends sensitively on  $\tilde{k}$ , characterizing the ratio of the natural frequency of the oscillator and the driving frequency, as well as on the dimensionless driving amplitude  $\tilde{g}$ , as depicted in Fig. 1b. In the regime of weak driving amplitude,  $|\tilde{g}| \lesssim 1$ , sharp unstable regions with strong heating,  $\text{Im}\nu(\tilde{k}, \tilde{g}) < 0$ , appear in the vicinity of the main resonance  $\tilde{k} = 1$ , satisfying the resonance condition (10), as well as around its higher harmonics  $\tilde{k} \in \mathbb{Z}$ . In particular, the unstable region around the main resonance  $\tilde{k} = 1$  extends to

$$1 - |\tilde{g}| < \tilde{k}^2 < 1 + |\tilde{g}|.$$

The higher-order resonances around  $\tilde{k} = 2, 3, \dots$  are weaker with a smaller  $|\text{Im}\nu(\tilde{k}, \tilde{g})|$ , thus the heating of these modes occurs on longer time scales than the heating of the main resonance. In contrast, in the regime of strong driving,  $|\tilde{g}| > 1$ , the resonances become very

broad, with large unstable regions displaying an exponential energy absorption. We note that a similar phase diagram holds in the more general case,  $J_0 > 0$ , with unstable lobes appearing around the main resonance and its higher harmonics,  $\varepsilon_k/\varepsilon_{k_{\text{res}}} \in \mathbb{Z}$ .

### III. DRIVING PROTOCOLS RETAINING THE GAP

In this section, we consider driving protocols that keep the gap open throughout the time evolution,  $J(t) > 0$  for all  $t$ . In this case we can compare TWA to the TDVP, which neglects the higher order correlations between modes and breaks down for driving protocols where the gap closes, i.e.  $J(t) = 0$  at certain times  $t$ . Therefore, we expect that TWA is better suited for examining the energy absorption of the system in the limit of strong modulation,  $J_1 > J_0$ . Nonetheless, TDVP can be used to benchmark our TWA results in certain limits.

#### A. Time-dependent variational principle

We briefly sketch the main ingredients of the time dependent variational principle (TDVP). Further details are relegated to the appendices, appendices B–E.

We consider the time-dependent sine-Gordon Hamiltonian density of Eq. (4),

$$\mathcal{H}[\varphi, \rho] = \frac{\pi c}{2K} \delta \rho^2 + \frac{cK}{2\pi} (\partial_x \varphi)^2 - 2J(t)\rho_0 \cos \varphi, \quad (14)$$

Here,  $\varphi(x)$  and  $\delta \rho(x) = -i\delta/\delta \varphi(x)$  satisfy the canonical commutation relation. Deep in the gapped phase, the ground state of the system can be well approximated by a Gaussian functional of the field  $\varphi(x)$ , localized near one of the minima of the cosine potential [42, 43]. In time-dependent problems starting from a localized state,  $\varphi$  remains localized as long as the gap is finite. The time evolution of the system can then be approximated by a time-dependent Gaussian wavefunction introduced by Cooper *et al.* [44]:

$$\Psi_v[\varphi(x)] = \mathcal{A} \exp \left( - \int_{x,y} \varphi(x) \left[ \frac{G_{x,y}^{-1}}{4} - i\Sigma_{x,y} \right] \varphi(y) \right). \quad (15)$$

Here  $G_{x,y}$  denotes the connected two-point correlator,

$$G_{x,y} = \langle \varphi(x) \varphi(y) \rangle - \varphi_{\text{cl}}(x) \varphi_{\text{cl}}(y),$$

where  $\varphi_{\text{cl}}(x)$  is the classical expectation value of the field,  $\langle \varphi(x) \rangle = \varphi_{\text{cl}}(x)$ . The correlator  $\Sigma_{x,y}$  corresponds to the conjugate function of  $G_{x,y}$ , and  $\mathcal{A} \sim (\det G)^{-1/4}$  is a normalization factor ensuring the unitarity of the evolution at all times,

$$\langle \Psi_v | \Psi_v \rangle = \int \mathcal{D}[\varphi] \Psi_v[\varphi]^* \Psi_v[\varphi] = 1. \quad (16)$$



The functions  $G_{x,y}, \Sigma_{x,y}$  constitute variational parameters that can be determined from the Dirac variational principle. To this end, it is convenient to define an effective classical Lagrangian density,

$$\mathcal{L}_{\text{cl}}[G_{x,y}, \Sigma_{x,y}, \varphi_{\text{cl}}(x), p_{\text{cl}}(x)] = \int \mathcal{D}[\varphi] \Psi_v[\varphi] (i\partial_t - \mathcal{H}[\varphi, \partial/\partial\varphi]) \Psi_v[\varphi]. \quad (17)$$

The equations of motion are obtained by making  $S_{\text{cl}} \equiv \int dt \int dx \mathcal{L}_{\text{cl}}$  stationary. For a translationally invariant system, it is convenient to perform a Fourier transformation,  $G_k \equiv \int_{-\Lambda}^{\Lambda} dk G_{x-y} e^{-ik(x-y)}$ , with  $\Lambda$  denoting a UV cutoff. A similar expression holds for  $\Sigma_k$ . After some algebra, the saddle point condition  $\delta S_{\text{cl}} = 0$  leads to the following equations of motion,

$$\dot{G}_k = \frac{4\pi c}{K} G_k \Sigma_k, \quad (18a)$$

$$\dot{\Sigma}_k = \frac{\pi c}{8K} G_k^{-2} - \frac{2\pi c}{K} \Sigma_k^2 - \frac{cK}{2\pi} k^2 - J(t) Z(t) \rho_0. \quad (18b)$$

Here the factor

$$Z(t) = \exp\left(-\frac{1}{2} \int_{-\Lambda}^{\Lambda} \frac{dk}{2\pi} G_k\right) \quad (19)$$

describes a renormalization of the tunnel coupling by the phase fluctuations. An equivalent Gaussian approximation for the dynamics can be obtained by replacing the time dependent variational principle arguments sketched above by an alternative [45, 46] self-consistent time dependent harmonic approximation (SCTDHA); see App. B. In that approach, the non-quadratic term  $-2J(t)\rho_0 \cos\varphi$  is replaced with  $-2J(t)\rho_0 \langle \cos\varphi \rangle (1 - \varphi^2/2)$ , making the operator equations of motion linear. The expectation value  $\langle \cos\varphi \rangle$  is then calculated self-consistently. We provide details on the equivalence of the two approaches in appendix C.

## B. Numerical results for gapped driving protocols

In this section we compare the TDVP to the semi-classical TWA for gapped driving protocols,  $J_1 < J_0$ . We note that the TDVP breaks down once the modulated Hamiltonian crosses a gapless point. Indeed, the closing of the gap amplifies the quantum fluctuations  $G_k$ , leading to the suppression of the renormalization factor,  $Z(t) \rightarrow 0$ , and ensuring that the gap remains closed for the rest of the time evolution. This effect is an artefact of the harmonic approximation. In the gapped regime  $J_1 < J_0$ , however, the quantum fluctuations can remain bounded, such that  $Z(t)$  stays finite at all times, and  $\varphi$  remains localized (see the appendix D for more details).

We consider the dynamics of the lattice Hamiltonian (8), starting from the approximate ground state of the system at  $t = 0$ , obtained by expanding the cosine function up to second order,  $\cos\varphi_i \approx 1 - \varphi_i^2$ . In the TDVP,

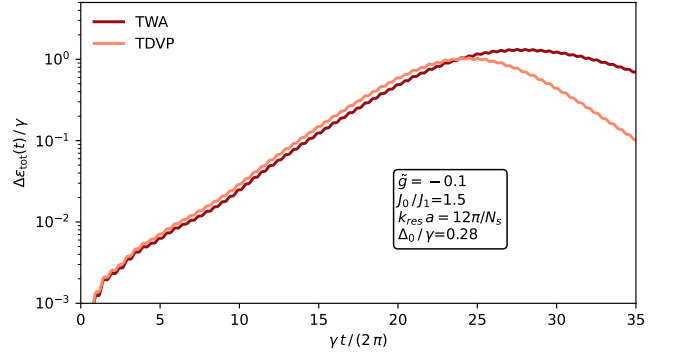


Figure 2. Parametric excitation of the sine-Gordon model in the gapped regime. We plot the absorbed total energy density  $\Delta\varepsilon_{\text{tot}}/\gamma$  of the static Hamiltonian on a log-linear scale as a function of rescaled time  $\gamma t/(2\pi)$ , obtained from the Truncated Wigner Approximation (TWA) and the Time-Dependent Variational Principle (TDVP). The energy absorption is exponentially fast up to intermediate times, but eventually gets suppressed due to the coupling between modes. The two approaches show a good agreement in the regime of exponential heating, but at longer times TDVP predicts a stronger suppression in the energy absorption due to the overestimation of the coupling renormalization. We used  $J_0/J_1 = 1.5$ ,  $N_s = 200$ ,  $K = 40$ ,  $\tilde{g} = -0.1$ ,  $k_{\text{res}} a = 12\pi/N_s$ , and  $\Delta_0/\gamma = 0.28$ .

this initial state corresponds to  $\Sigma_k(t = 0) = 0$  and

$$G_k(t = 0) = \frac{\pi}{2K} \frac{1}{\sqrt{4c^2/a^2 \sin^2(ka/2) + \Delta_0^2}}, \quad (20)$$

with the approximate gap  $\Delta_0$  given by Eq. (6). We focus on the total energy density of the static Hamiltonian,

$$\varepsilon_{\text{tot}}(t) = \frac{\langle H_{\text{stat}} \rangle(t)}{N_s},$$

where the static component  $H_{\text{stat}}$  is obtained by replacing  $J(t) \rightarrow J_0$  in Eq. (8).

We set the driving frequency to satisfy the parametric resonance condition Eq. (10) for one of the low energy modes  $k_{\text{res}}$ , and study the energy absorption  $\Delta\varepsilon_{\text{tot}}(t) = \varepsilon_{\text{tot}}(t) - \varepsilon_{\text{tot}}(0)$  using the TDVP and TWA approaches. The TDVP result is obtained by solving Eqs. (18) numerically, with initial conditions specified by Eq. (20). The Wigner distribution of the initial state, required for the TWA method, is also determined by Eq. (20), resulting in a Gaussian distribution for the initial phase and particle number fluctuations.

The results are shown in Fig. 2 for a moderate modulation strength  $\tilde{g} = -0.1$ , tunnel coupling ratio  $J_0/J_1 = 1.5$ , and static gap  $\Delta_0/\gamma = 0.28$ . The parametric resonance leads to an exponentially fast energy absorption at short and intermediate time scales, and we find a good agreement between the TWA and TDVP results in this regime. At longer times, however, the coupling between modes leads to the suppression of the energy absorption

in the system. At these time scales the higher order correlations between modes become relevant, and the Gaussian TDVP yields a stronger suppression compared to TWA, where such correlations are incorporated to the time evolution.

#### IV. DRIVING PROTOCOLS CLOSING THE GAP

In this section we turn to modulations in the regime  $J_1 > J_0$ , resulting in the closing of the instantaneous gap during the time evolution. Here, we rely solely on TWA simulations, because the TDVP approach breaks down for these driving protocols. For simplicity, we focus on  $J_0 = 0$ , such that the static Hamiltonian is a quadratic Luttinger liquid, convenient for studying the mode resolved energy absorption of different modes  $k$ . First we discuss the heating in the main resonance, satisfying Eq. (10), and its higher harmonics in Sec. IV A. Then we present a simple toy model capturing the most relevant coupling terms in Sec. IV B, and tests its predictions in Sec. IV C.

##### A. Heating of main resonance and its higher harmonics

The Mathieu equation (12), describing the dynamics of the sine-Gordon model up to linear order, predicts sharp resonances for a parametric drive satisfying the resonance condition (10) around the main resonance and its higher harmonics,  $\tilde{k} \in \mathbb{Z}$ , for weak driving amplitude  $|\tilde{g}| < 1$ . To test these predictions, and to identify the effect of non-linear mode couplings in the full many-body dynamics, we investigate the mode-resolved energy absorption of the sine-Gordon model, by applying TWA. As before, we focus on the lattice-regularized model, Eq. (8), where the modulated tunnel coupling  $J(t)$  is given by Eq. (9) with  $J_0 = 0$ . This Hamiltonian is quadratic at  $t = 0$ , and we initialize the system in its ground state.

The quadratic part of the lattice Hamiltonian (8) can be easily diagonalized by Fourier transformation, yielding the spectrum

$$\varepsilon_k = \frac{2c}{a} \left| \sin \frac{ka}{2} \right|, \quad (21)$$

reducing to the linear Luttinger-liquid spectrum (5) for small wave numbers  $k \ll 1/a$ . We tune the driving frequency to parametric resonance with one of the low-energy modes according to Eq. (10), and consider the energy absorption of different modes,

$$E_k(t) = c \left( \frac{\pi}{2Ka} \langle n_k n_{-k} \rangle(t) + \frac{2K}{\pi a} \sin^2 \frac{ka}{2} \langle \varphi_k \varphi_{-k} \rangle(t) \right). \quad (22)$$

Here, we defined  $n_k = 1/\sqrt{N_s} \sum_j n_j e^{-ijak}$ , with a similar relation for  $\varphi_k$ . We can then apply the semi-classical

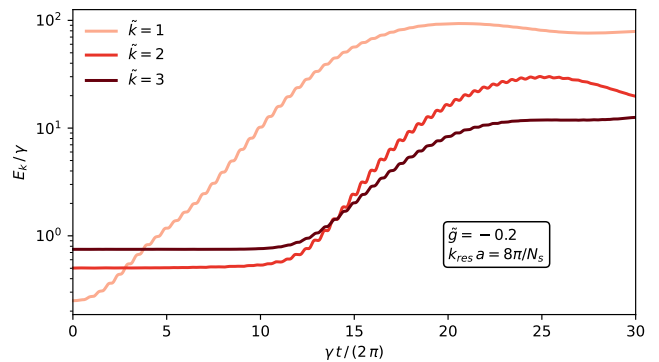


Figure 3. Parametric excitation of the resonant mode and its higher harmonics. We plot the energy  $E_k$  on a log-linear scale as a function of rescaled time  $\gamma t/(2\pi)$  for modes  $k \equiv k/k_{\text{res}} = 1, 2, 3$ . The main resonance  $\tilde{k} = 1$  shows an exponentially fast energy absorption due to the external parametric drive. The energy absorption in higher harmonics is suppressed on short time scales, but crosses over to an intermediate exponential increase at later times, due to an effective drive provided by the non-linear coupling to the highly-excited main resonance. We used  $N_s = 200$ ,  $K = 40$ ,  $\tilde{g} = -0.2$ , and  $k_{\text{res}} a = 8\pi/N_s$ .

truncated Wigner approximation [32], for evaluating the mode-resolved energy, Eq. (22), as a function of time. Below we parametrize the modes by the dimensionless wave number introduced in Sec. II A,  $\tilde{k} \equiv k/k_{\text{res}}$ .

We plot the energy Eq. (22) for the main resonance  $\tilde{k} = 1$ , as well as the higher harmonics  $\tilde{k} = 2$  and  $\tilde{k} = 3$  as a function of time in Fig. 3 for a moderate modulation strength  $\tilde{g} = -0.2$ . We find exponentially fast energy absorption in the main resonance  $\tilde{k} = 1$  already at early times, in accordance with the linear Mathieu equation discussed in Sec. II B. At later times, the energy saturates due to the strong coupling to other modes. However, the heating of the higher harmonics  $\tilde{k} = 2$  and  $\tilde{k} = 3$  differs substantially from the dynamics of uncoupled oscillators. In contrast to a higher order parametric resonance, displaying a steady, albeit slow, heating, the energy absorption in modes  $k = 2$  and  $k = 3$  is almost completely suppressed at early times. Then we observe a crossover to an unstable regime with exponentially fast heating at intermediate times, followed by an eventual saturation at even later times. This peculiar behavior is a consequence of the mode-coupling in the driven sine-Gordon Hamiltonian.

##### B. Simplified model for mode-coupling

In order to identify the most relevant coupling terms between modes, and to shed more light to the results shown above, we present a simplified toy model for the dynamics, focusing on the main resonance and its higher harmonics. To this end, we consider Eq. (11), and apply the expansion  $\sin \varphi_j \approx \varphi_j - \varphi_j^3/6$ , thereby keeping the

lowest order non-linearity in the equation of motion. By applying a Fourier transformation and changing to the dimensionless variables introduced in Sec. IIB, we obtain

$$\left(\partial_\tau^2 + \tilde{k}^2 - 2\tilde{g}\sin(2\tau)\right)\varphi_{\tilde{k}} = -\frac{\tilde{g}}{6N_s}\sin(2\tau)\sum_{\tilde{k}_1, \tilde{k}_2}\varphi_{\tilde{k}_1}\varphi_{\tilde{k}_2}\varphi_{\tilde{k}-\tilde{k}_1-\tilde{k}_2}. \quad (23)$$

From our numerical results we conclude that the energy absorption at short and intermediate times is dominated by the main resonance and a few higher harmonics for weak drives. Therefore, we keep only the resonant indices  $\tilde{k} \in \mathbb{Z}$  in Eq. (23) and drop the others. We focus on the dynamics of the two lowest harmonics  $\tilde{k} = 2$  and  $\tilde{k} = 3$ , and identify the most important coupling terms on the right hand side of Eq. (23).

Since the main resonance  $\tilde{k} = 1$  is the mode with the largest heating rate, on short times scales the coupling to this mode will provide the dominant contribution to the energy absorption of the second harmonics  $\tilde{k} = 2$ . These considerations lead to the following equation of motion for mode  $\tilde{k} = 2$ ,

$$(\partial_\tau^2 + 4 - 2\tilde{g}\sin(2\tau))\varphi_2 = -\frac{\tilde{g}}{N_s}\sin(2\tau)|\varphi_1|^2\varphi_2. \quad (24)$$

As noted in Sec. IIB, the linear Mathieu equation for  $\tilde{k} = 2$  gives rise to a weak resonance for  $|\tilde{g}| \lesssim 1$  (left hand side of Eq. (24)). The mode heats up exponentially as a function of time, however, the time scale associated with this heating is much longer than the typical time scale of energy absorption for the main resonance,  $\tilde{k} = 1$ . Consequently, the contribution from this direct resonance is negligible at the early and intermediate stages of the dynamics. In contrast, we find that the non-linear coupling term on the right hand side gives rise to an effective resonant parametric drive for mode  $\tilde{k} = 2$ , and leads to a fast heating. Note that the time dependence of this driving term is determined by  $\sin(2\tau)|\varphi_1|^2$ . In our units, the natural frequency of mode  $\tilde{k} = 1$  is 1, thus the average  $\langle |\varphi_1|^2 \rangle$  contains an oscillating contribution  $\sim \cos(2\tau)$ . Combining this with the external modulation  $\sin(2\tau)$ , we arrive at an effective parametric drive  $\sim \sin(4\tau)\varphi_2$ . By comparing to the resonance condition, Eq. (10), we find that this drive satisfies the parametric resonance condition, giving rise to a strong first order resonance, accompanied by an exponentially fast heating for mode  $\tilde{k} = 2$ . Importantly, the amplitude of this effective drive depends on the occupation of the main resonance through the amplitude  $|\varphi_1|^2$ , leading to a weaker effect at short time scales, but becoming dominant at intermediate times, once mode  $\tilde{k} = 1$  has sufficiently heated up. We present the detailed numerical solution of Eq. (24) in Appendix F.

Since lower harmonics are expected to display a larger heating rate for mode  $\tilde{k} = 3$ , we identify the following dominant non-linear coupling terms, coupling  $k = 3$  to

modes  $\tilde{k} = 1$  and  $\tilde{k} = 2$ ,

$$(\partial_\tau^2 + 9 - 2\tilde{g}\sin(2\tau))\varphi_3 = -\frac{\tilde{g}}{N_s}\sin(2\tau)(|\varphi_1|^2 + |\varphi_2|^2)\varphi_3 - \frac{\tilde{g}}{6N_s}\sin(2\tau)\varphi_1^3. \quad (25)$$

The first two terms on the right hand side give rise to effective parametric drives, whereas the last term acts as an external driving force for mode  $\tilde{k} = 3$ . The first effective parametric drive,  $\sim \sin(2\tau)|\varphi_1|^2$ , becomes stronger rapidly due to the exponentially fast heating of mode 1, and starts to induce an efficient energy absorption in mode  $\tilde{k} = 3$  at intermediate time scales. The second parametric drive,  $\sim \sin(2\tau)|\varphi_2|^2$ , contains terms oscillating as  $\sin(2\tau)\cos(4\tau) \sim \sin(6\tau)$ , satisfying the resonance condition (10) for mode  $\tilde{k} = 3$ , and leading to a first order parametric resonance. Similarly to the effective resonant drive identified for mode  $\tilde{k} = 2$ , the amplitude of the drive depends on the heating of a lower-lying mode. Therefore, the heating rate induced by this coupling becomes larger at intermediate time scales, when the occupation of the lower mode is sufficiently large. Finally, the third term on the right hand side of Eq. (25) amounts to an external driving force. Here  $\varphi_1^3$  gives rise to oscillating terms of the form  $e^{\pm 3i\tau}$  and  $e^{\pm i\tau}$ , leading to an effective resonant drive  $\sin(2\tau)e^{\pm i\tau} \sim e^{\pm 3i\tau}$  for mode  $\tilde{k} = 3$ . While a resonant external force with constant amplitude gives rise to a heating that is linear in time, the force provided by mode  $\tilde{k} = 1$  increases exponentially with time, as mode  $\tilde{k} = 1$  becomes more populated. Therefore, this term contributes considerably to the exponentially fast heating of mode  $\tilde{k} = 3$  at intermediate time scales, similarly to the effective parametric drives discussed above.

Our simplified model provides a qualitative explanation for the results plotted in Fig. 3. At short times, the main resonance starts to heat up exponentially fast due to the external parametric drive. In contrast, the direct energy absorption of the higher harmonics  $\tilde{k} > 1$  from the external drive is much less efficient, moreover, the non-linear coupling to mode  $\tilde{k} = 1$  is still weak due to the low population of this mode. Therefore, the heating of modes  $\tilde{k} > 1$  remains suppressed on short time scales. At intermediate time scales, the coupling between mode  $\tilde{k} = 1$  and its higher harmonics becomes dominant due to the high population of the main resonance. The strong effective parametric drive and external driving force emerging from this coupling give rise to an exponentially fast heating in modes  $\tilde{k} = 2$  and  $\tilde{k} = 3$ . Finally, at even later times the population of all of these modes saturates due to the coupling to the bath formed by the remaining modes. For more details, see Appendix F.

Even though the simplified model yields a qualitative explanation for the results plotted in Fig. 3, it does not capture the almost perfect suppression of heating in modes  $\tilde{k} = 2$  and  $\tilde{k} = 3$  at short time scales, instead predicting a slow decrease in energy (see Appendix F). This deviation between the simplified description and the full quantum model is a direct consequence of the difference between the expansion  $\sin \varphi \approx \varphi - \varphi^3/6$ , and the exact

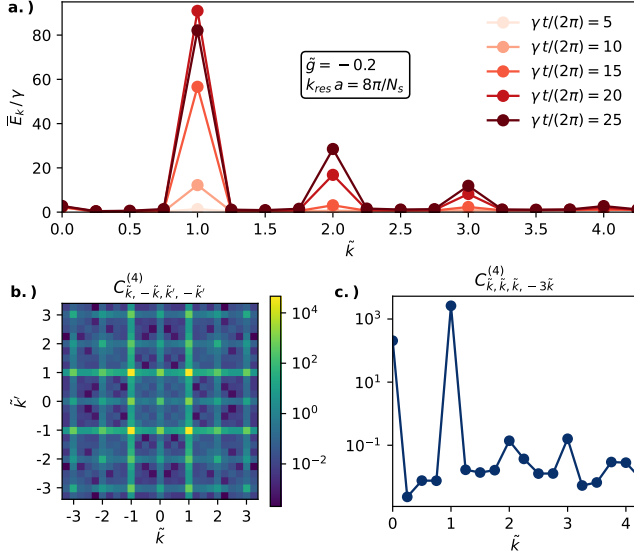


Figure 4. Energy profile and correlations for a weak drive. **a.)** Snapshots of the energy profile  $\bar{E}_k$ , averaged over one driving period, for different times, displaying sharp peaks at the main resonance and its higher harmonics. Exponential heating in the main resonance starts immediately, whereas the absorption in higher-order resonances is strongly suppressed at short times. At later times sharp peaks also emerge at the higher harmonics, as they absorb energy from the highly-excited main resonance. **b.)** Higher-order correlations between modes obtained from the connected correlator  $C_{k,-k,k',-k'}^{(4)}$  as a function of dimensionless wave numbers  $\tilde{k} = k/k_{\text{res}}$  and  $\tilde{k}' = k'/k_{\text{res}}$ . **c.)** Higher-order correlators  $C_{k,k,k,-3k}^{(4)}$  as a function of  $\tilde{k}$ , averaged over one driving period at time  $\gamma t/(2\pi) = 12.5$ . The correlator  $C_{k,-k,k',-k'}^{(4)}$  displays strong correlations between the main resonance and the higher harmonics,  $\tilde{k} \in \mathbb{Z}, \tilde{k}' \in \mathbb{Z}$ , while  $C_{k,k,k,-3k}^{(4)}$  reveals a sharp correlation peak between modes 1 and -3. We used  $N_s = 200$ ,  $K = 40$ ,  $\tilde{g} = -0.2$ , and  $k_{\text{res}} a = 8\pi/N_s$ .

function  $\sin \varphi$  appearing in the mean field equation of motion, pointing towards the importance of the precise form of the many-body potential in the dynamics.

### C. Distribution of absorbed energy and higher-order correlations

We examine the heating of different modes, as well as the higher order correlations in the system for weak driving amplitude in Fig 4. This allows us to test the predictions of the simplified model presented in the previous section in more detail. We will briefly comment on the case of stronger modulations at the end of the section.

To cancel the rapid oscillations stemming from the external drive, we average the energy over one period of the

drive,

$$\bar{E}_k(t) = \frac{1}{T} \int_{t-T/2}^{t+T/2} dt' E_k(t'), \quad (26)$$

with  $T = 2\pi/\gamma$ . We plot snapshots of the mode-dependent energy  $\bar{E}_k$  at different times for a weak driving amplitude  $\tilde{g} = -0.4$  in Fig 4a. As anticipated in Sec. IV B, the heating at short and intermediate time scales is dominated by the main resonance and its higher harmonics, leading to sharp peaks in the energy at wave numbers  $\tilde{k} \in \mathbb{Z}$ . In accordance with the delay of the heating in higher harmonics discussed above, the resonance peaks around  $\tilde{k} = 2$  and  $\tilde{k} = 3$  remain strongly suppressed on short time scales, and become more pronounced at later times.

To further investigate the scope of the effective description discussed in Sec. IV B, we also examine the higher-order density correlations in the system. We consider two different fourth-order correlation functions,

$$C_{k,-k,k',-k'}^{(4)} = \langle n_k n_{-k} n_{k'} n_{-k'} \rangle_c, \quad (27)$$

and

$$C_{k,k,k,k}^{(4)} = \langle n_k^3 n_k \rangle_c, \quad (28)$$

with  $\langle \dots \rangle_c$  standing for a connected correlator, and  $n_k$  denoting the Fourier transform of the particle number operator,  $n_k = 1/\sqrt{N_s} \sum_j n_j e^{-ijak}$ . Due to translation invariance,  $C_{k,k,k,k}^{(4)}$  is non-zero only for  $k' = -3k$ , whereas  $C_{k,-k,k',-k'}^{(4)}$  can be finite for arbitrary wave numbers  $k$  and  $k'$ . Similarly to Eq. (26), we average these correlators over one period of the drive.

We show snapshots of the averaged correlators  $C_{k,-k,k',-k'}^{(4)}$  and  $C_{k,k,k,-3k}^{(4)}$  at an intermediate time  $\gamma t/(2\pi) = 12.5$ , in the regime of weak modulation,  $|\tilde{g}| \lesssim 1$ , in Fig 4b and c. We find that  $C_{k,-k,k',-k'}^{(4)}$  displays sharp correlation peaks between the multiples of the resonant mode,  $\tilde{k} \in \mathbb{Z}, \tilde{k}' \in \mathbb{Z}$ . This behavior can be understood based on the simplified equations (24) and (25). The effective parametric drive appearing on the right hand side of these equations induces strong correlations of the type  $C_{k,-k,k',-k'}^{(4)}$  between the main resonance and the higher harmonics,  $\tilde{k}, \tilde{k}' \in \mathbb{Z}$ , in accordance with the results plotted in Fig 4b. By contrast, the correlator  $C_{k,k,k,-3k}^{(4)}$  reveals strong correlations between  $n_{-3\tilde{k}}$  and  $n_{\tilde{k}}^3$  for the main resonance  $\tilde{k} = 1$ , as well as much weaker correlation peaks for the higher harmonics  $\tilde{k} = 2$  and  $\tilde{k} = 3$  (see Fig 4c). The sharp correlation peak at  $\tilde{k} = 1$  is consistent with the effective driving force appearing on the right hand side of Eq. (25), providing a strong coupling between the operators  $\varphi_1^3$  and  $\varphi_{-3}$ .

In the presence of a large driving amplitude  $|\tilde{g}| > 1$ , the heating dynamics is modified. We plot the mode-resolved energy profile  $\bar{E}_k(t)$  for different times in Fig. 5,



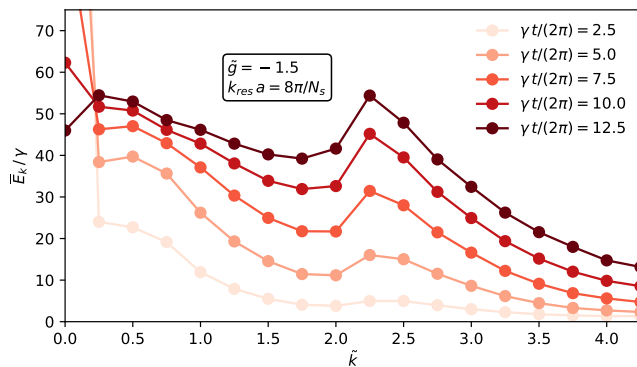


Figure 5. Energy profile for strong drive. Snapshots of the energy profile  $\bar{E}_k$  for different times, averaged over one driving period, for a large modulation  $\tilde{g} = -1.5$ . The broadening of the parametric resonance and the strong coupling between modes leads to a smoother energy profile than the one obtained for weak drives  $|\tilde{g}| \lesssim 1$ . The threshold  $\tilde{k}_{\text{thres}} \approx 2.25$  separates a broad region with fast heating from the more stable modes with slower energy absorption. We used  $N_s = 200$ ,  $K = 40$ , and  $k_{\text{res}} a = 8\pi/N_s$ .

using the driving strength  $\tilde{g} = -1.5$ . In contrast to the case of a weak drive discussed above, a strong modulation leads to a broad parametric resonance, as well as to strong non-linear couplings between modes, resulting in a smoother energy profile  $E_k$  at all times, without well defined resonance peaks. Instead, we observe a threshold at  $\tilde{k}_{\text{thres}} \approx 2.25$ , above which the energy starts to fall off as a function of  $\tilde{k}$ . We can gain a qualitative understanding of this behavior based on the uncoupled Mathieu equations (12), predicting a broadened first and second resonance in close proximity. The mode-coupling modifies the boundary of these unstable lobes, merging them into a single broad heating region  $\text{Im } \nu(\tilde{k}, \tilde{g}) < 0$  with exponentially fast heating below the threshold  $\tilde{k}_{\text{thres}}$ . While this perturbative reasoning explains the main features in Fig. 5, the details of the dynamics depend strongly on the pronounced coupling between the modes, and can only be obtained from a simulation accounting for the full many-body potential.

For the strong drive considered in Fig. 5, the homogeneous mode  $k = 0$  heats up exponentially fast, with a large heating rate, giving rise to a pronounced peak on short time scales (compare to the phase diagram of a single oscillator, Fig. 1). At later times, this high excitation is transferred to the remaining modes, as can be observed in Fig. 5.

## V. OUTLOOK AND EXPERIMENTAL IMPLICATIONS

We have considered a quantum many-body analogue of a classical parametric oscillator, the sine-Gordon model in the presence of a modulated cosine potential. For weak

driving amplitudes, we have found an exponentially fast heating of the main resonance, whereas the energy absorption of the higher-order resonances is suppressed on short time scales. On longer time scales the non-linear coupling terms in the Hamiltonian excite higher-order resonances by effective parametric drives as well as external driving forces generated from the highly excited main resonance. Such mode coupling allow the higher resonances to absorb energy from the highly excited main resonance and gives rise to further sharp resonance peaks in the mode-resolved energy density. We have identified the most relevant couplings by exploring the higher-order correlations between modes, and constructed a simplified model to explain our findings. While this model provides a good qualitative understanding for our main results, it fails to describe some aspects of the dynamics, such as the almost perfect suppression of energy absorption at short times in all modes except the main resonance. This indicates the relevance of the full many-body potential in the time evolution.

The modulated tunnel coupling can be experimentally realized two parallel quasi-one-dimensional condensates in the presence of a modulated tunnel coupling. The one-dimensional description of this system, Eq. (1), fails when the transverse modes of the double well potential cannot be neglected anymore. At late times, these transverse modes may become populated due to the strong heating, leading to deviations from the sine-Gordon description. For the parameters used in this work, the total energy density of the system remains small compared to the chemical potential  $gN$ , with  $N$  denoting the total particle number (despite some modes being exponentially populated). Under these conditions, we expect that the transverse modes of the trap can be neglected on the time scales we consider.

While realizing an oscillating coupling of the form of Eq. (9) with a deformed double well potential is relatively straightforward in the regime  $J_1 < J_0$ , reversing the sign of  $J(t)$  is substantially more challenging. We propose the procedure schematically depicted in Fig. 6 to realize the tunnel coupling  $J(t) = J_1 \sin(\gamma t)$ . The first half-period,  $0 \leq t \leq \pi/\gamma$ , can be realized by deforming the double-well trapping potential. An effective sign change can then be implemented by changing the global phase difference,  $\varphi_1 - \varphi_2$ , of the now uncoupled condensates by  $\pi$ . In the absence of tunnel coupling,  $J(t) = 0$ , the phase difference  $\pi$  can be imprinted by switching on an energy difference  $\epsilon$  between the two condensates, by adding a small left-right asymmetry to the double well trapping potential [7, 26]. The energy difference results in a global phase accumulation  $\Delta(\varphi_1 - \varphi_2) = \epsilon t$ , reaching the desired value  $\pi$  at time  $t = \pi/\epsilon$ . Once the phase  $\pi$  has been imprinted, the energy difference  $\epsilon$  can be switched off. Repeating the same modulation sequence,  $J(t) = J_1 \sin(\gamma t)$ ,  $0 \leq t \leq \pi/\gamma$ , leads to a time-dependent cosine potential with an opposite sign,  $-J(t) \cos(\varphi_j + \pi) = J(t) \cos \varphi_j$ , completing the first driving cycle.

We note that we have performed our simulations with

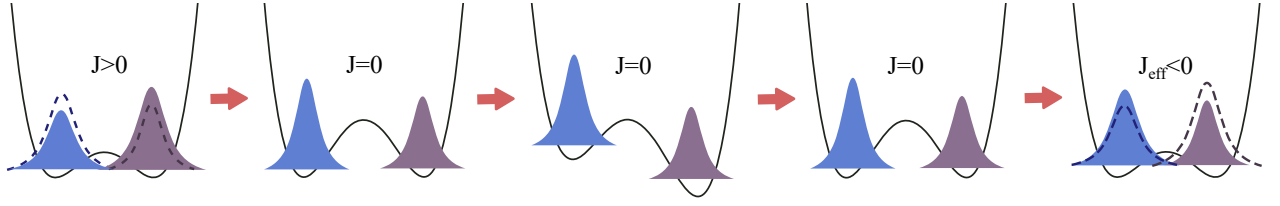


Figure 6. Proposed experimental protocol. The driven sine-Gordon model is experimentally accessible with quasi-one-dimensional condensates in a double-well potential, coupled through a modulated Josephson tunneling term. A tunnel-coupling oscillating around zero mean can be realized as follows: In the first half-period, the tunnel coupling is modulated as  $J(t) = J_1 \sin(\gamma t)$ ,  $0 \leq t \leq \pi/\gamma$ . Upon reaching  $J(t) = 0$ , the sign of the tunneling is reversed by implementing a global phase rotation  $\pi$ , through switching on a left-right asymmetry in the trapping potential. Once the desired phase difference  $\pi$  has been imprinted, the asymmetry is switched off. Repeating after this rotation the same half-period  $J(t) = J_1 \sin(\gamma t)$ ,  $0 \leq t \leq \pi/\gamma$ , results in an effective tunnel coupling  $J_{\text{eff}}(t) = -J_1 \sin(\gamma t)$ , completing the driving cycle.

periodic boundary conditions, amounting to a homogeneous average density and phase,  $\langle n_k \rangle = \langle \varphi_k \rangle = 0$ . We were able to detect the parametric instability by examining the time-dependent correlators  $\langle n_k n_{-k} \rangle(t)$  and  $\langle \varphi_k \varphi_{-k} \rangle(t)$  (compare to Eq. (22)), as well as the higher-order correlators Eqs. (27) and (28). An experimental realization corresponds to open boundary conditions, and the parametric heating gives rise to a modulated density and phase pattern, with  $\langle n_k \rangle(t)$  and  $\langle \varphi_k \rangle(t)$  increasing rapidly for  $k$  close to resonance. Therefore, in realistic experimental settings, the parametric resonance, and the correlation patterns arising from the mode-coupling can be detected from the average density, and from the second order correlation functions, such as  $\langle n_k n_{k'} \rangle(t)$ .

Besides the experimental relevance of our results, studying the mode-resolved energy absorption of other slowly driven quantum many-body systems remains of interest. The distribution of the absorbed energy, and the emerging correlation patterns can shed light on the dominant coupling terms between quasi-particles, as well as on the role of conservation laws or kinetic constraints.

**Acknowledgements.** We thank Jörg Schmiedmayer for insightful discussions. We acknowledge support from the Deutsche Forschungsgemeinschaft (DFG, German Research Foundation) under Germany's Excellence Strategy-EXC-2111-390814868, TRR80 and DFG grants No. KN1254/1-2 and No. KN1254/2-1, the European Research Council (ERC) under the European Union's Horizon 2020 research and innovation programme (grant agreements No. 851161 and 771537), as well as the Munich Quantum Valley, which is supported by the Bavarian state government with funds from the Hightech Agenda Bayern Plus. This work was supported by the Gordon and Betty Moore Foundation through Grant GBMF8690 to UCSB, by the Harvard-MIT CUA, AFOSR-MURI award FA95501610323, the ARO grant "Control of Many-Body States Using Strong Coherent Light-Matter Coupling in Terahertz Cavities", and by the Swiss National Science Foundation under Division II.

## Appendix A: Derivation of the bosonized Hamiltonian

Using the notations of Ref. 36, the low energy excitations of the decoupled Hamiltonian (1) are described by the bosonized Hamiltonian

$$H_0 = \sum_{j=1,2} \int \frac{dx}{2\pi} \left[ u_* K_* (\pi \Pi_j)^2 + \frac{u_*}{K_*} (\partial_x \phi_j)^2 \right],$$

where  $u_*$  is the velocity of excitations,  $K_*$  the Luttinger parameters,  $[\phi_j(x), \Pi_k(x')] = i\delta_{jk}\delta(x-x')$ . As a result of Galilean invariance[35],

$$u_* K_* = \frac{\pi \rho_0}{m},$$

while  $K_*/u_*$  can be obtained from the compressibility of the Lieb-Liniger model. For weak coupling, we have the approximations

$$u_* \simeq \sqrt{\frac{\rho_0 g}{m}},$$

$$K_* \simeq \pi \sqrt{\frac{\rho_0}{mg}}.$$

The time dependent Josephson tunneling term (2) has the bosonized expression

$$H_J = -2J(t)\rho_0 \int dx \cos(\theta_1 - \theta_2)(x),$$

with  $\partial_x \theta_j = \pi \Pi_j$ . It is convenient to introduce symmetric and antisymmetric combinations

$$\phi_r = \frac{1}{\sqrt{2}}(\phi_1 + r\phi_2), \theta_r = \frac{1}{\sqrt{2}}(\theta_1 + r\theta_2)$$

with  $r = \pm$ , and rewrite  $H = H_+ + H_-$  with

$$H_+ = \int \frac{dx}{2\pi} \left[ u_* K_* (\pi \Pi_+)^2 + \frac{u_*}{K_*} (\partial_x \phi_+)^2 \right],$$

$$H_- = \int \frac{dx}{2\pi} \left[ u_* K_* (\pi \Pi_-)^2 + \frac{u_*}{K_*} (\partial_x \phi_-)^2 \right]$$

$$-2J(t)\rho_0 \int \cos \sqrt{2}\theta_-,$$

We now introduce  $\varphi = -\sqrt{2}\theta_-$  and  $n = -\partial_x\phi_-/\sqrt{2}$ . In order to discretize, we replace  $\partial_x\varphi$  with  $(\varphi_{j+1} - \varphi_j)/a$  and  $n(ja)$  with  $n_j/a$ . We end up with

$$H_- = \sum_j \left[ \frac{u_* K_*}{4\pi a} (\varphi_{j+1} - \varphi_j)^2 + \frac{\pi u_*}{a K_*} n_j^2 - 2J(t)\rho_0 a \cos \varphi_j \right],$$

leading to Eq. (8) with  $c = u_*$  and  $K = K_*/2$ .

## Appendix B: Alternative formulation of SCTDHA for the Frenkel-Kontorova model

In this appendix we present an alternative formulation of the time dependent self-consistent harmonic approximation for the Frenkel-Kontorova model, following the approach described in Refs. [45, 46]. As shown in App. C, this approximation is equivalent to the time-dependent variational principle described in Sec. III A.

This approach relies on approximating the cosine term of the Frenkel-Kontorova model (8) as

$$\cos \varphi_j \simeq e^{-\frac{\langle \varphi_j^2 \rangle}{2}} \left( 1 - \frac{\varphi_j^2}{2} \right),$$

such that

$$H_{Lat} \simeq \frac{c}{2} \sum_{j=1}^{N_s} \left[ \frac{\pi n_j^2}{Ka} + \frac{K}{\pi a} (\varphi_{j+1} - \varphi_j)^2 + \rho_0 J(t) a Z(t) \varphi_j^2 \right], \quad (\text{B1})$$

with  $Z(t) = e^{-\langle \varphi_j^2 \rangle(t)/2}$ .

It is convenient to use the Fourier decomposition

$$n_j = \frac{1}{\sqrt{N_s}} \sum_k n_k e^{ikj},$$

$$\varphi_j = \frac{1}{\sqrt{N_s}} \sum_k \varphi_k e^{ikj},$$

where  $k = \frac{2\pi p}{N_s}$  with  $p$  integer, and to rewrite Eq.(B1) as

$$H_{Lat} = \frac{c}{2} \sum_k \left\{ \frac{\pi n_k n_{-k}}{Ka} + \left[ \frac{2K}{\pi a} (1 - \cos k) + \rho_0 J(t) a Z(t) \right] \varphi_k \varphi_{-k} \right\}.$$

We obtain the equation of motion

$$\frac{d^2 \varphi_k(t)}{dt^2} + [\omega_k^2 + \Omega^2(t)] \varphi_k(t) = 0, \quad (\text{B2})$$

with

$$\omega_k^2 = \frac{2c^2}{a^2} (1 - \cos ka),$$

$$\Omega^2(t) = \frac{2\pi c \rho_0 J(t) Z(t)}{K}.$$

The time evolution of  $\varphi_k(t)$  is fully determined by Eq. (B2) and the knowledge of  $\varphi_k(0)$  and

$$\left( \frac{d\varphi_k(t)}{dt} \right)_{t=0} = \frac{\pi c n_k(0)}{Ka}. \quad (\text{B3})$$

Those initial conditions are determined by the ground state of the initial Hamiltonian. Since we have set  $\Delta(t < 0) = \Delta(0)$ ,

$$H_{SCTDHA}(t < 0) = \sum_k \sqrt{\omega_k^2 + \Omega^2(0)} (a_k^\dagger a_k + 1/2),$$

with

$$\varphi_k = \frac{a_{-k}^\dagger + a_k}{\sqrt{\frac{2Ka}{\pi c} \sqrt{\omega_k^2 + \Omega^2(0)}}},$$

$$n_k = i \sqrt{\frac{Ka}{\pi c} \sqrt{\omega_k^2 + \Omega^2(0)}} \frac{a_{-k}^\dagger - a_k}{\sqrt{2}}.$$

Using these expressions and requiring that  $Z(t)$  should be determined self-consistently from Eq. (B1), we obtain a set of differential equations for each  $k$ ,

$$\frac{d^2 Y_k}{dt^2} + \left[ \omega_k^2 + \frac{2\rho_0 \pi c J(t) Z(t)}{K} \right] Y_k = 0, \quad (\text{B4})$$

with initial condition

$$Y_k(0) = \frac{1}{(\omega_k^2 + \Omega^2(0))^{1/4}},$$

$$\dot{Y}_k(0) = -i(\omega_k^2 + \Omega^2(0))^{1/4}. \quad (\text{B5})$$

Finally, the coupling renormalization  $Z(t)$  is determined by

$$Z(t) = \exp \left[ -\frac{\pi c}{4N_s K a} \sum_k |Y_k(t)|^2 \right]. \quad (\text{B6})$$

Therefore, the equation giving  $Z(t)$  is reduced to a non-linear differential equation for the vector  $Y_k(t)$  with initial conditions given by (B5). Such equation can be integrated numerically with the Runge-Kutta algorithm (see [47] p. 897). The numerical solution of  $Y_k(t)$  will be discussed in more detail below.

To fully determine the initial condition, we have to solve for  $\Omega(0)$ . The selfconsistent equation is

$$\frac{a^2 \Omega^2(0)}{c^2} = \frac{2\pi \rho_0 J(0) a^2}{cK} \times \exp \left[ -\frac{\pi}{4N_s K} \sum_k \frac{1}{\sqrt{4 \sin^2(ka/2) + (a\Omega/c)^2(0)}} \right]. \quad (\text{B7})$$

When  $K > \frac{1}{8}$ , Eq. (B7), has solutions for  $J(0) \ll c/(\rho_0 a^2)$  with

$$\Omega(0) = \frac{2\pi c}{a} \left( \frac{\rho_0 J(0) a^2}{2\pi c K} \right)^{\frac{4K}{8K-1}},$$

$$Z(0) = \left( \frac{\rho_0 J(0) a^2}{2\pi c K} \right)^{\frac{1}{8K-1}}.$$

If we assume that  $Z(t)$  is almost constant, the conditions to find resonant modes will be

$$\omega^2(k_*) + \int_0^T \frac{dt}{T} \frac{2\pi\rho_0 c Z(0)}{K} J(t) = \frac{n^2 \gamma^2}{4},$$

with  $n \geq 1$  integer, so for

$$\gamma > 2\sqrt{\omega^2(\pi) + \int_0^T \frac{dt}{T} \frac{2\pi\rho_0 c Z(0)}{K} J(t)}, \quad (\text{B8})$$

resonant modes are absent. In such case of high frequency driving,  $Z(t)$  can reach a non-zero limit at long times. However, when the condition (B8) is not satisfied, an unstable mode growing exponentially will be present, leading to  $Z(t) \rightarrow 0$ . Thus, the approximation of constant  $Z(t)$  breaks down over a timescale determined by the Floquet exponent with the largest imaginary part. Besides, the previous argument also shows that at long times, when  $\gamma < 2\omega(\pi)$ ,  $Z(t)$  cannot have a strictly positive limit. Otherwise, we would find an exponentially growing mode leading to  $Z(t) \rightarrow 0$  and a contradiction. Thus, we are lead to expect two regimes, one of high frequency driving with  $Z(t)$  approaching a finite limit at long times, and another of low frequency driving with  $Z(t)$  going to zero for long times. In App. B2, we consider a simplified model, where only the resonant modes are taken into account. The model shows some periodic revivals of the coherence; albeit with a duration that decreases as  $O(1/t)$ .

### 1. Numerical results for renormalization term $Z(t)$

Assuming for a moment that  $Z(t)$  is given, we consider the linear differential equation

$$\frac{d^2 Y_k}{dt^2} + [\omega_k^2 + \Omega^2(t)] Y_k(t) = 0,$$

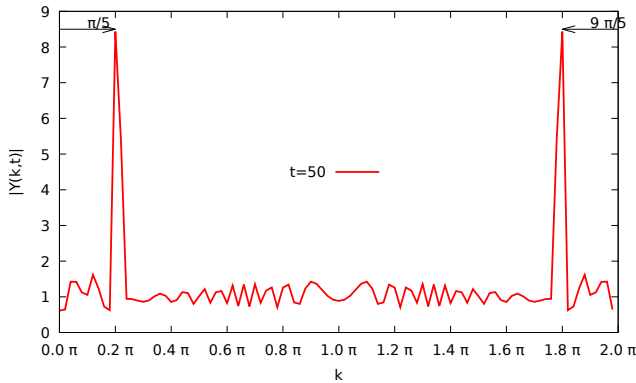


Figure 7. Plot of the modulus of  $Y_k(t)$  versus  $k$  at time  $t = 50$ . The two resonant modes at  $k^* = \frac{\pi}{5}$  and  $2\pi - k^*$  are clearly visible.

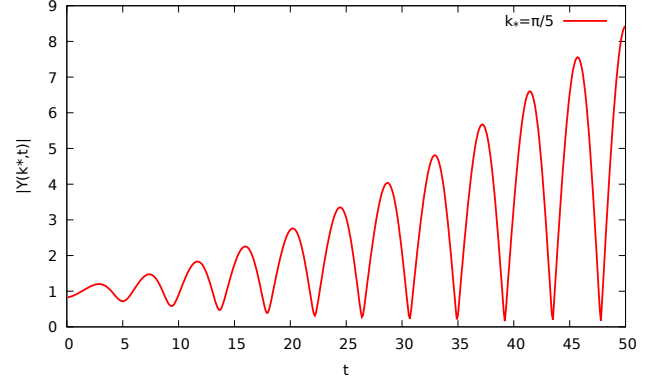


Figure 8. Plot of  $|Y(k^*, t)|$  as a function of time. The amplitude of the oscillations is increasing with time.

and its fundamental solutions

$$\begin{pmatrix} y_1 & y_2 \\ \dot{y}_1 & \dot{y}_2 \end{pmatrix} (k, t=0) = \begin{pmatrix} 1 & 0 \\ 0 & 1 \end{pmatrix}.$$

We find that

$$\varphi_k(t) = \frac{1}{(2\frac{Ka}{\pi c} \sqrt{\omega_k^2 + \Omega^2(0)})^{1/2}} \left[ a_k (y_1 - i\sqrt{\omega_k^2 + \Omega^2(0)} y_2) + a_{-k}^\dagger (y_1 + i\sqrt{\omega_k^2 + \Omega^2(0)} y_2) \right],$$

resulting in

$$Z(t) = \exp \left[ -\frac{\pi c}{4NKa} \sum_k \frac{y_{1k}(t)^2 + y_{2k}(t)^2 (\omega_k^2 + \Omega^2(0))}{\sqrt{\omega_k^2 + \Omega^2(0)}} \right].$$

We have solved numerically the differential equation for  $Z(t)$  and  $Y_k(t)$  for  $J(t) = J_0 + J_1 \cos(\gamma t)$ , where  $\gamma T = 2\pi$ . We have picked our unit of time so that  $c/a = 1$  and set  $K = \pi$ . We show the results for the case of  $J_0 = J_1 = 0.1$  and  $\gamma = 1.5$ . In figure 7, the modulus of  $Y_k(t)$  is plotted as a function of  $k$ . We have resonant modes at  $k^* = \pi/5$  and  $2\pi - k^* = 9\pi/5$ .

The time evolution of the resonant mode is shown on Fig. 8. The amplitude is not a monotonous function of time, but shows a succession of maxima and minima, with the height of the maxima increasing with time.

Plotting the maxima as a function of time on a semi-logarithmic scale (Fig. 9), we find the points are close to a straight line, compatible with exponential growth at short times.

### 2. Analytical results for the self-consistent time-dependent harmonic approximation

We now discuss a few analytical approximations derived within the SCTDHA. For the differential equation (B4) we can show that for each  $k$ ,

$$Y_k^*(t) \frac{dY_k(t)}{dt} - Y_k(t) \frac{dY_k^*(t)}{dt} = -2i,$$



and we have energy conservation

$$\begin{aligned} & \frac{d}{dt} \left( \sum_k \left| \frac{dY}{dt} \right|^2 (k, t) + \omega_k^2 |Y_k(t)|^2 - 8\Delta(t)Z(t) \right) \\ &= -8N \frac{d\Delta}{dt} Z(t), \end{aligned} \quad (\text{B9})$$

where  $\Delta(t) = \rho_0 a J(t)$ . After integrating (B9) over time, we find that if there is at least one mode  $Y(k \neq 0, t)$  whose amplitude grows to infinity, then

$$\int_0^{+\infty} Z(t) \frac{d\Delta}{dt} dt = -\infty,$$

and since  $0 < Z(t) < 1$  while  $\Delta(t)$  is also bounded,

$$\int_0^{+\infty} \Delta(t) \frac{dZ}{dt} dt = +\infty.$$

Using

$$\begin{aligned} & \left| \int_0^t Z(t') \frac{\Delta}{dt'} \right| < \int_0^t Z(t) \left| \frac{\Delta}{dt} \right| < \\ & < \text{Max}_{0 < t < T} \left| \frac{d\Delta}{dt} \right| \int_0^t Z(t') dt', \end{aligned}$$

so if we have modes with a divergent amplitudes,

$$\int_0^{+\infty} Z(t) dt = +\infty.$$

Eq. (B6), however, implies that having modes with divergent amplitudes leads to  $Z(t) \rightarrow 0$ . So  $Z(t)$  should decay to zero sufficiently slowly at long times to yield a divergent integral, implying that the amplitudes of unstable modes  $|Y(k, t)|$  are also growing sufficiently slowly. Now, let's return to Eq. (B4), with  $J(t)$  given by Eq. (9), and let's consider  $k = k_r$  where  $\omega(k_r) = \gamma/2$ . We will seek  $Y(k_r, t)$  in the form

$$Y(k_r, t) = A(t)e^{i\frac{\gamma}{2}t} + B(t)e^{-i\frac{\gamma}{2}t},$$

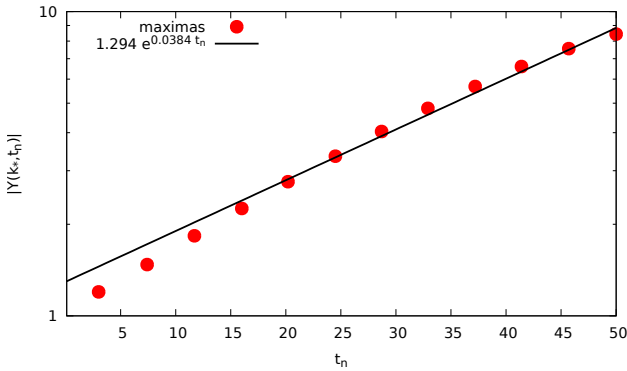


Figure 9. Plot of  $|Y_{k*}(t_{max,n})|$  versus  $t_{max,n}$  on semi-logarithmic scale. This can be fitted by an exponential.

neglecting  $2\pi\rho_0 c J_0 Z(t)/K$  compared with  $\gamma^2/4$ . We end up with the system of differential equations,

$$\begin{aligned} & \frac{d^2 A}{dt^2} + i\gamma \frac{dA}{dt} - i \frac{\pi\rho_0 c J_1}{K} Z(t) B = 0, \\ & \frac{d^2 B}{dt^2} - i\gamma \frac{dB}{dt} + i \frac{\pi\rho_0 c J_1}{K} Z(t) A = 0. \end{aligned}$$

Neglecting the second derivatives, as  $A(t)$  and  $B(t)$  are expected to vary slowly over one period, and introducing Pauli matrices, we rewrite our system as

$$i\gamma\sigma_3 \begin{pmatrix} A \\ B \end{pmatrix} + \frac{\pi\rho_0 c J_1}{K} Z(t)\sigma_2 \begin{pmatrix} A \\ B \end{pmatrix} = 0,$$

that is solved in the form

$$\begin{pmatrix} A(t) \\ B(t) \end{pmatrix} = \exp \left[ \int_{t_0}^t \frac{\pi\rho_0 c J_1}{\gamma K} \sigma_1 Z(t') dt' \right] \begin{pmatrix} A(t_0) \\ B(t_0) \end{pmatrix}.$$

We see that when the integral of  $Z$  is finite,  $A$  and  $B$  remain finite, but if the integral of  $Z$  is divergent,  $A$  and  $B$  will grow to infinity. With the help of (B2), we find

$$Y(k_r, t) = \mathcal{A} \cos \left( \frac{\gamma t}{2} \right) \exp \left[ \int_0^t \frac{\pi\rho_0 c J_1}{\gamma K} Z(t') dt' \right] + \dots$$

The same equation holds for  $Y(-k_r, t)$ . The amplitude squared diverges as

$$|Y(k_r, t)|^2 = \frac{|\mathcal{A}|^2}{2} [1 - \cos \gamma t] \exp \left[ \int_0^t \frac{2\pi\rho_0 c J_1}{\gamma K} Z(t') dt' \right] + \dots,$$

and we have

$$\begin{aligned} & \left| \frac{dY(k_r, t)}{dt} \right|^2 + \frac{\gamma^2}{4} |Y(k_r, t)|^2 = \\ & \frac{\gamma^2 |\mathcal{A}|^2}{4} \exp \left[ \int_0^t \frac{2\pi\rho_0 c J_1}{\gamma K} Z(t') dt' \right]. \end{aligned} \quad (\text{B10})$$

Assuming only the modes at  $\pm k_r$  are divergent, and introducing

$$\zeta(t) = \frac{\pi c |\mathcal{A}|^2}{4N K a} \exp \left[ \int_0^t \frac{2\pi\rho_0 c J_1}{\gamma K} Z(t') dt' \right], \quad (\text{B11})$$

we obtain

$$\frac{\dot{\zeta}}{\zeta} = \frac{2\pi\rho_0 c J_1}{\gamma K} \exp [-(1 - \cos \gamma t)\zeta(t)].$$

We have the inequality

$$\int^{\zeta(t)} \frac{d\zeta'}{\zeta'} e^{2\zeta'} \geq \frac{2\pi J_1 \rho_0 c t}{\gamma K},$$

yielding

$$\zeta(t) \geq \frac{1}{2} \ln \left[ \frac{2\pi J_1 \rho_0 c t}{\gamma K} \ln \left( \frac{2\pi J_1 \rho_0 c t}{\gamma K} \right) \right] + o(1).$$

Since  $\zeta(t) \rightarrow +\infty$ , Eq. (B2) implies that except in the vicinity of  $\gamma t = 2n\pi$ , with integer  $n$ ,  $\dot{\zeta} \ll 1$ . Near  $\gamma t = 2n\pi$ , we can expand the cosine in Eq. (B2) to obtain

$$\frac{\dot{\zeta}}{\zeta} \simeq e^{-\zeta(2n\pi/\gamma)(\gamma t - 2n\pi)^2/2}.$$

$$\zeta\left(\frac{2n}{\gamma}\right) \exp\left[\frac{\pi\rho_0 c J_1}{\gamma^2 K} \sqrt{\frac{2\pi}{\zeta\left(\frac{2n}{\gamma}\right)}}\right] = \zeta\left(\frac{2n+2}{\gamma}\right) \exp\left[-\frac{\pi\rho_0 c J_1}{\gamma^2 K} \sqrt{\frac{2\pi}{\zeta\left(\frac{2n+2}{\gamma}\right)}}\right].$$

We can rewrite this equation in differential form to arrive at

$$\zeta\left(\frac{2n}{\gamma}\right) \simeq 2\pi \left(\frac{n\pi\rho_0 c J_1}{\gamma^2 K}\right)^2,$$

and for  $(2n-1)\pi < \gamma t < (2n+1)\pi$ ,

$$\zeta(t) \simeq 2\pi \left(\frac{n\pi\rho_0 c J_1}{\gamma^2 K}\right)^2 \times \exp\left\{\frac{1}{2n} \operatorname{erf}\left[\frac{2\pi^{3/2}\rho_0 c J_1}{\gamma K} n \left(t - \frac{2n\pi}{\gamma}\right)\right]\right\},$$

and

$$Z(t) \simeq \exp\left[-\pi \left(\frac{\pi\rho_0 c J_1 n}{\gamma K}\right)^2 \left(t - 2n\frac{\pi}{\gamma}\right)^2\right],$$

We thus obtain

$$\int_{\frac{(2n-1)\pi}{\gamma}}^{\frac{(2n+1)\pi}{\gamma}} dt Z(t) \simeq \frac{\gamma K}{\pi\rho_0 c J_1 n},$$

and

$$\int_0^t dt Z(t) \sim \frac{\gamma K}{\pi\rho_0 c J_1} \ln \frac{\gamma t}{2\pi}.$$

Qualitatively, at long times,  $Z(t)$  is nearly zero except in intervals of size  $\sim 1/n$  around  $t = 2n\pi/\gamma$ , where  $Z(t) \simeq 1$ . This leads to short lived periodic revivals of the phase coherence between the chains. The non-resonant modes lead to a blurring of those revivals, but spikes in  $Z(t)$  are visible in our numerical simulations. If we consider

By integrating, we have the relations

$$\begin{aligned} \zeta\left(\frac{2n+1}{\gamma}\right) &\simeq \zeta\left(\frac{2n}{\gamma}\right) \exp\left[\frac{\pi\rho_0 c J_1}{\gamma^2 K} \sqrt{\frac{2\pi}{\zeta\left(\frac{2n}{\gamma}\right)}}\right], \\ \zeta\left(\frac{2n-1}{\gamma}\right) &\simeq \zeta\left(\frac{2n}{\gamma}\right) \exp\left[-\frac{\pi\rho_0 c J_1}{\gamma^2 K} \sqrt{\frac{2\pi}{\zeta\left(\frac{2n}{\gamma}\right)}}\right], \end{aligned}$$

provided  $\zeta(2n\pi) \gg 1$ . Using the above expressions to obtain  $\zeta[(2n+1)\pi/\gamma]$  as a function of  $\zeta[2n\pi/\gamma]$  and of  $\zeta[(2n+2)\pi/\gamma]$ , we get

the total energy,  $\Delta(t)Z(t)$  is bounded, so it is enough to use (B10) to find the energy going as

$$\begin{aligned} \langle H(t) \rangle &\sim \frac{2Na}{cK} \left(\frac{\pi\rho_0 c J_1 n}{\gamma}\right)^2 \times \\ &\exp\left\{\frac{1}{2n} \operatorname{erf}\left[\frac{2\pi^{3/2}\rho_0 c J_1}{\gamma K} n \left(t - \frac{2n\pi}{\gamma}\right)\right]\right\}, \end{aligned}$$

when  $t \sim 2n\pi$ . We find an energy increasing as  $O(t^2)$ .

### Appendix C: Equivalence of the time-dependent variational principle and the self-consistent time dependent harmonic approximation

In this appendix we show the equivalence of the time-dependent variational principle outlined in Sec. III A, and the time dependent self-consistent harmonic approximation as formulated in Refs.[45, 46] and used in App. B.

First, expressing  $\Sigma_k$  as a function of  $\dot{G}_k/G_k$ , the system (18) is rewritten as a single second order differential equation for  $G_k$

$$\frac{K}{4\pi c} \left[ \frac{\ddot{G}_k}{G_k} - \frac{1}{2} \left( \frac{\dot{G}_k}{G_k} \right)^2 \right] = \frac{\pi c}{8K G_k^2} - \frac{cK}{2\pi} k^2 - J(t)Z(t)\rho_0. \quad (C1)$$

Introducing  $y_k = \sqrt{G_k}$ , one has

$$\frac{1}{y_k} \frac{d^2 y_k}{dt^2} = \frac{1}{2} \left[ \frac{\ddot{G}_k}{G_k} - \frac{1}{2} \left( \frac{\dot{G}_k}{G_k} \right)^2 \right],$$

so that in terms of  $y_k$ , Eq. (C1) becomes

$$\frac{d^2 y_k}{dt^2} = \frac{(\pi c)^2}{4K^2 y_k^3} - \left( c^2 k^2 + \frac{2\pi c J(t) Z(t) \rho_0}{K} \right) y_k. \quad (C2)$$

Eq. (C2) is the equation of motion of a classical particle moving in a time-dependent harmonic central force field written in polar coordinates[30]. The term  $\pi^2 c^2 / (4K^2 y_k^3)$  is the centrifugal force, while the term proportional to  $y_k$  is the harmonic restoring force. Eq. (C2) is thus linearized by introducing the angular coordinate  $\theta_k$  satisfying

$$\frac{d\theta_k}{dt} = \frac{\pi c}{2K y_k^2}. \quad (\text{C3})$$

with initial condition  $\theta_k(0) = 0$ . In terms of the variable  $z_k = \sqrt{G_k} e^{i\theta_k}$ , Eq. (C2) becomes

$$\frac{d^2 z_k}{dt^2} = \left( c^2 k^2 + \frac{2\pi c J(t) Z(t) \rho_0}{K} \right) z_k. \quad (\text{C4})$$

That is precisely Eq. (B4), obtained using the self-consistent time dependent harmonic approximation (SCTDHA) [45, 46].

Having reduced Eq. (18) to a linear second order equation, the initial conditions of Eq. (C4) are

$$\begin{aligned} z_k(0) &= \sqrt{G_k(0)} \\ \dot{z}_k(0) &= \frac{2\pi c}{K} \sqrt{G_k(0)} \Sigma_k(0) + \frac{i\pi c}{2K \sqrt{G_k(0)}}. \end{aligned}$$

Again using the solutions  $y_{1k}(t)$  and  $y_{2k}(t)$  of the differential equation

$$\frac{d^2 Y_k}{dt^2} = - \left( c^2 k^2 + \frac{2\pi c J(t) Z(t) \rho_0}{K} \right) Y_k,$$

with initial conditions

$$\begin{pmatrix} y_1(0) & y_2(0) \\ \dot{y}_1(0) & \dot{y}_2(0) \end{pmatrix} = \begin{pmatrix} 1 & 0 \\ 0 & 1 \end{pmatrix},$$

we find

$$z_k(t) = \sqrt{G_k(0)} \left[ y_{1k}(t) + \frac{2\pi c}{K} \Sigma_k(0) y_{2k}(t) + \frac{i\pi c y_{2k}(t)}{2K G_k(0)} \right].$$

Since our initial state was a steady state,  $\Sigma_k(0) = 0$ . Then,  $G_k(t) = |z_k(t)|^2$  yields

$$G_k(t) = G_k(0) \left[ y_{1k}(t)^2 + \frac{\pi^2 c^2 y_{2k}(t)^2}{4K^2 G_k(0)^2} \right],$$

and using the equilibrium Green's function Eq. (20), we get

$$\begin{aligned} Z(t) &= \\ \exp \left[ - \int_{-\Lambda}^{\Lambda} \frac{dk}{8K \sqrt{k^2 + \Delta_0^2}} (y_{1k}(t)^2 + c^2 (k^2 + \Delta_0^2) y_{2k}(t)^2) \right]. \end{aligned}$$

#### Appendix D: Gap renormalization and infinite temperature runaway instability in SCTDHA in the amplitude-modulated sine-Gordon model

In Sec. III we approximated the gap of the sine-Gordon model with  $J_0 \neq 0$  by Eq. (7). A more precise expression within SCTDHA takes into account the renormalization of the tunnel coupling by quantum fluctuations. To this end, the system is assumed to be in its stationary gapped ground state, i.e.  $\Sigma_k = 0$  for  $t \leq 0$ . The initial correlator for the continuum version is determined from Eq. (18b),

$$G_k = \frac{\pi}{2K} \frac{1}{\sqrt{k^2 + \Delta_0^2}},$$

where  $\Delta_0$  is self-consistently given as:

$$\Delta_0^2 = \frac{2\pi J \rho_0}{cK} \exp \left( - \frac{1}{2} \int_{-\Lambda}^{\Lambda} \frac{dk}{4K} \frac{1}{\sqrt{k^2 + \Delta_0^2}} \right).$$

Assuming  $\Delta_0 \ll \Lambda$ , the above equation gives  $\Delta_0^2 \approx (g_0/2) [\Delta_0/(2\Lambda)]^{1/(4K)}$ , which implies that  $K_c = \frac{1}{8}$  (Kosterlitz-Thouless transition). The cosine is relevant (irrelevant) for  $K > K_c$  ( $K < K_c$ ). In this initial gapped phase, the classical oscillation frequency,  $\sqrt{g_0}$  is renormalized by the factor  $Z$  due to quantum fluctuations.

In the presence of a modulation in the tunnel coupling, the system can enter a region of infinite temperature runaway instability depending on the strength and frequency of the modulation. This effect can be understood within the variational wavefunction approach as follows. In the initial gapped phase, the classical oscillation frequency near the  $\varphi = 0$  minimum of the cosine potential is renormalized by the factor  $Z$  due to quantum fluctuations. The introduction of a modulation to the amplitude of the bare cosine potential can give rise to an ergodic regime which amplifies quantum fluctuations (i.e. leads to “particle generation” via parametric resonance) and closes the gap, i.e.  $Z(t) \rightarrow 0$ . Once the gap closes, it remains closed; we take this as an indication of the runaway to the infinite-temperature limit. For weaker modulations, however, the system can stay in a non-ergodic regime, where the quantum fluctuations remains bounded,  $Z(t)$  remains finite at all times, and  $\varphi$  remains localized. The phase diagram showing the ergodic-non-ergodic phase transition was previously derived in Ref. 15.

### Appendix E: Adiabatic limit in the selfconsistent time dependent harmonic approximation

If we make a WKB approximation[48] in Eq. (B2), we find:

$$y_{1k}(t) = \left( \frac{\omega_k^2 + \Omega^2(0)}{\omega_k^2 + \Omega^2(t)} \right)^{1/4} \cos \left[ \int_0^t \sqrt{\omega_k^2 + \Omega^2(t')} dt' \right],$$

$$y_{2k}(t) = \frac{(\omega_k^2 + \Omega^2(0))^{-1/4}}{(\omega_k^2 + \Omega^2(t))^{1/4}} \sin \left[ \int_0^t \sqrt{\omega_k^2 + \Omega^2(t')} dt' \right],$$

and substituting this expression into (B6) gives

$$\Omega(t) = \frac{2\pi c}{a} \left( \frac{\rho_0 a^2 J(t)}{2\pi c K} \right)^{\frac{4K}{8K-1}}.$$

In the adiabatic regime, the modes adapt instantaneously to the variations of the hopping  $J(t)$  and the evolution of the gap is adiabatic. Now, when  $J(t+T) = J(t)$  is periodic,  $\Omega(t) = \Omega(t+T)$ . The WKB solutions (E1) can then be combined as  $y_1 \pm i(\omega_k^2 + \Omega^2(0))^{1/2} y_2$  to satisfy a Floquet condition with Floquet exponent

$$\pi\nu(k) = \pm \int_0^T \sqrt{\omega_k^2 + \Omega^2(t)} dt.$$

The condition for the validity of the WKB approximation is

$$\left| \frac{d}{dt} (\sqrt{\omega_k^2 + \Omega^2(t)}) \right| \ll \omega_k^2 + \Omega^2(t),$$

so it is always valid for  $\omega_k \gg \dot{\Omega}$ . For  $k \rightarrow 0$ , the condition becomes

$$\left| \frac{d\Omega}{dt} \right| \ll \Omega^2(t). \quad (\text{E1})$$

In the case of a periodic  $\Omega(t) > 0$ , Eq. (E1) imposes  $\gamma < \min_{0 < t < T} \Omega(t)$ . The resonance condition being  $\sqrt{\omega_k^2 + \Omega^2} = n\gamma/2$ , the only possible resonances are at  $n \gg 1$  and their width and Lyapunov exponent are exponentially suppressed with  $\Omega/\gamma$ . This explains the purely real Floquet exponents in the adiabatic limit. Eq. (E1) also indicates that adiabaticity breaks down when  $\Omega(t) \rightarrow 0$ . In the case of  $J(t) = \lambda(t_0 - t)$ , we enter a non-adiabatic regime at  $t = t_*$  with

$$t_0 - t_* \sim \frac{a}{c} \left( \frac{c^2 K}{\rho_0 a^3 \lambda} \right)^{\frac{4K}{12K-1}}. \quad (\text{E2})$$

In particular the modes with momenta  $k < k_* \sim (\rho_0 a^3 \lambda / c^2)^{\frac{4K}{12K-1}}$  start to exhibit non-adiabatic evolution. But since the timescale  $t_0 - t_*$  is less than one period of these modes, they behave as if they had been frozen at time  $t = t_*$ . As a result,  $\langle \cos \varphi_j \rangle(t_0) = Z(t_*) \sim \lambda^{\frac{1}{12K-1}}$  indicating a residual coherence.

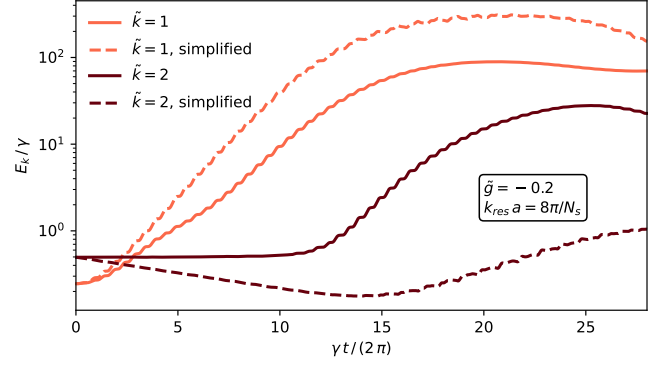


Figure 10. Simplified description of heating. We compare the absorption predicted by the simplified equations (F1) and (F2) (dashed) to the full TWA time evolution (solid) for modes  $\tilde{k} \equiv k/k_{\text{res}} = 1, 2$ . We plot the energy  $E_k$  on a log-linear scale as a function of rescaled time  $\gamma t / (2\pi)$ . For the main resonance  $\tilde{k} = 1$ , Eq. (F1) predicts a faster heating than TWA, due to the absence of coupling to other modes. For the higher harmonics  $\tilde{k} = 2$ , Eq. (F2) yields an initial energy decrease. At later times, however, the emergent parametric drive provided by the main resonance gives rise to an exponential heating, albeit with a smaller rate than the one from the TWA solution. We used  $N_s = 200$ ,  $K = 40$ ,  $\tilde{g} = -0.2$ , and  $k_{\text{res}} a = 8\pi/N_s$ .

### Appendix F: Numerical results for the simplified model of mode coupling

In this appendix we present numerical results calculated from the simplified model for mode coupling, presented in Sec. IV B. We focus on the main resonance  $\tilde{k} = 1$  and on the first higher harmonics  $\tilde{k} = 2$ , and compare the numerical solution of the simplified equations,

$$(\partial_\tau^2 + 1 - 2\tilde{g} \sin(2\tau)) \varphi_1 = -\frac{\tilde{g}}{2N_s} \sin(2\tau) |\varphi_1|^2 \varphi_1 \quad (\text{F1})$$

and

$$(\partial_\tau^2 + 4 - 2\tilde{g} \sin(2\tau)) \varphi_2 = -\frac{\tilde{g}}{N_s} \sin(2\tau) |\varphi_1|^2 \varphi_2, \quad (\text{F2})$$

to the full TWA solution for a moderate coupling strength  $\tilde{g} = -0.2$ . The results are plotted in Fig. 10. For the main resonance  $\tilde{k} = 1$ , Eq. (F1) yields a larger heating rate than the full TWA solution, because we neglect the coupling and energy transfer to other modes. For the higher harmonics  $\tilde{k} = 2$ , Eq. (F2) gives a decreasing energy at early times, whereas the energy of the mode remains approximately constant in the full TWA. At later times, the coupling to the main resonance becomes dominant, giving rise to an exponentially fast energy absorption. The heating rate, however, is considerably smaller than the rate obtained from the TWA simulations.

While the simplified equations (F1) and (F2) can not account for all details of the full TWA dynamics, they are able to capture some important qualitative features,



and illustrate how the coupling to the main resonance in-

duces exponentially fast heating in the higher harmonics as discussed in the main text.

- 
- [1] I. Bloch, J. Dalibard, and W. Zwerger, Many-body physics with ultracold gases, *Rev. Mod. Phys.* **80**, 885 (2008).
  - [2] T. Langen, R. Geiger, and J. Schmiedmayer, Ultracold atoms out of equilibrium, *Annual Review of Condensed Matter Physics* **6**, 201 (2015), <https://doi.org/10.1146/annurev-conmatphys-031214-014548>.
  - [3] C. Gross and I. Bloch, Quantum simulations with ultracold atoms in optical lattices, *Science* **357**, 995 (2017), <https://science.sciencemag.org/content/357/6355/995.full.pdf>.
  - [4] J. Cuevas-Maraver, P. G. Kevrekidis, and F. Williams, eds., *The Sine-Gordon Model and its Applications*, Springer Series in Nonlinear Systems and Complexity, Vol. 10 (Springer, 2014).
  - [5] V. Gritsev, A. Polkovnikov, and E. Demler, Linear response theory for a pair of coupled one-dimensional condensates of interacting atoms, *Phys. Rev. B* **75**, 174511 (2007).
  - [6] T. Schweigler, V. Kasper, S. Erne, I. Mazets, B. Rauer, F. Cataldini, T. Langen, T. Gasenzer, J. Berges, and J. Schmiedmayer, Experimental characterization of a quantum many-body system via higher-order correlations, *Nature* **545**, 323 (2017).
  - [7] M. Pigneur, T. Berrada, M. Bonneau, T. Schumm, E. Demler, and J. Schmiedmayer, Relaxation to a phase-locked equilibrium state in a one-dimensional bosonic josephson junction, *Phys. Rev. Lett.* **120**, 173601 (2018).
  - [8] T. Schweigler, M. Gluza, M. Tajik, S. Sotiriadis, F. Cataldini, S.-C. Ji, F. S. Møller, J. Sabino, B. Rauer, J. Eisert, and J. Schmiedmayer, Decay and recurrence of non-gaussian correlations in a quantum many-body system, *Nature Physics* **17**, 559 (2021).
  - [9] V. Kasper, J. Marino, S. Ji, V. Gritsev, J. Schmiedmayer, and E. Demler, Simulating a quantum commensurate-incommensurate phase transition using two raman-coupled one-dimensional condensates, *Phys. Rev. B* **101**, 224102 (2020).
  - [10] L. Foini and T. Giamarchi, Nonequilibrium dynamics of coupled luttinger liquids, *Phys. Rev. A* **91**, 023627 (2015).
  - [11] P. Ruggiero, L. Foini, and T. Giamarchi, Large-scale thermalization, prethermalization, and impact of temperature in the quench dynamics of two unequal luttinger liquids, *Phys. Rev. Research* **3**, 013048 (2021).
  - [12] E. Wybo, M. Knap, and A. Bastianello, *Quantum sine-gordon dynamics in coupled spin chains* (2022), [arXiv:2203.09530](https://arxiv.org/abs/2203.09530).
  - [13] A. Iucci, M. A. Cazalilla, A. F. Ho, and T. Giamarchi, Energy absorption of a bose gas in a periodically modulated optical lattice, *Phys. Rev. A* **73**, 041608 (2006).
  - [14] R. Citro, E. Demler, T. Giamarchi, M. Knap, and E. Orignac, Lattice modulation spectroscopy of one-dimensional quantum gases: Universal scaling of the absorbed energy, *Phys. Rev. Research* **2**, 033187 (2020).
  - [15] R. Citro, E. G. Dalla Torre, L. D'Alessio, A. Polkovnikov, M. Babadi, T. Oka, and E. Demler, Dynamical stability of a many-body kapitza pendulum, *Annals of Physics* **360**, 694 (2015).
  - [16] M. Bukov, S. Gopalakrishnan, M. Knap, and E. Demler, Prethermal floquet steady states and instabilities in the periodically driven, weakly interacting bose-hubbard model, *Physical Review Letters* **115**, 205301 (2015).
  - [17] A. Chandran and S. L. Sondhi, Interaction-stabilized steady states in the driven o(n) model, *Physical Review B* **93**, 174305 (2016).
  - [18] S. A. Weidinger and M. Knap, Floquet prethermalization and regimes of heating in a periodically driven, interacting quantum system, *Scientific Reports* **7**, 45382 (2017).
  - [19] A. Herrmann, Y. Murakami, M. Eckstein, and P. Werner, Floquet prethermalization in the resonantly driven hubbard model, *EPL (Europhysics Letters)* **120**, 57001 (2017).
  - [20] S. Lellouch, M. Bukov, E. Demler, and N. Goldman, Parametric instability rates in periodically driven band systems, *Phys. Rev. X* **7**, 021015 (2017).
  - [21] T. Boulier, J. Maslek, M. Bukov, C. Bracamontes, E. Magnan, S. Lellouch, E. Demler, N. Goldman, and J. V. Porto, Parametric heating in a 2d periodically driven bosonic system: Beyond the weakly interacting regime, *Phys. Rev. X* **9**, 011047 (2019).
  - [22] K. Wintersperger, M. Bukov, J. Näger, S. Lellouch, E. Demler, U. Schneider, I. Bloch, N. Goldman, and M. Aidelsburger, Parametric instabilities of interacting bosons in periodically driven 1d optical lattices, *Phys. Rev. X* **10**, 011030 (2020).
  - [23] C. Kuhlenskamp and M. Knap, Periodically driven sachdev-ye-kitaev models, *Physical Review Letters* **124**, 106401 (2020).
  - [24] M. Albiez, R. Gati, J. Fölling, S. Hunsmann, M. Cristiani, and M. K. Oberthaler, Direct observation of tunneling and nonlinear self-trapping in a single bosonic josephson junction, *Phys. Rev. Lett.* **95**, 010402 (2005).
  - [25] S. Levy, E. Lahoud, I. Shomroni, and J. Steinhauer, The a.c. and d.c. josephson effects in a bose-einstein condensate, *Nature* **449**, 579 (2007).
  - [26] T. Berrada, S. van Frank, R. Bücke, T. Schumm, J.-F. Schaff, and J. Schmiedmayer, Integrated mach-zehnder interferometer for bose-einstein condensates, *Nature Communications* **4**, 2077 (2013).
  - [27] Y. Zhang, G. Chen, and C. Zhang, Tunable spin-orbit coupling and quantum phase transition in a trapped bose-einstein condensate, *Scientific Reports* **3**, 1937 (2013).
  - [28] C. Hamner, Y. Zhang, M. A. Khomehchi, M. J. Davis, and P. Engels, Spin-orbit-coupled bose-einstein condensates in a one-dimensional optical lattice, *Phys. Rev. Lett.* **114**, 070401 (2015).
  - [29] A. J. Olson, S.-J. Wang, R. J. Niffenegger, C.-H. Li, C. H. Greene, and Y. P. Chen, Tunable landau-zener transitions in a spin-orbit-coupled bose-einstein condensate, *Phys. Rev. A* **90**, 013616 (2014).
  - [30] L. D. Landau and E. M. Lifshitz, *Mechanics: Volume 1*, Vol. 1 (Butterworth-Heinemann, 1976).

- [31] V. I. Arnold, *Geometrical Methods in the Theory of Ordinary Differential Equations*, Grundlehren der mathematischen Wissenschaften, Vol. 250 (Springer-Verlag, 1988).
- [32] A. Polkovnikov, Phase space representation of quantum dynamics, *Annals of Physics* **325**, 1790 (2010).
- [33] M. A. Cazalilla, Bosonizing one-dimensional cold atomic gases, *Journal of Physics B: Atomic, Molecular and Optical Physics* **37**, S1 (2004).
- [34] V. Gritsev, A. Polkovnikov, and E. Demler, Linear response theory for a pair of coupled one-dimensional condensates of interacting atoms, *Phys. Rev. B* **75**, 174511 (2007).
- [35] F. D. M. Haldane, Effective harmonic-fluid approach to low-energy properties of one-dimensional quantum fluids, *Phys. Rev. Lett.* **47**, 1840 (1981).
- [36] T. Giamarchi, *Quantum Physics in One Dimension*, International Series of Monographs in Physics, Oxford University Press (Clarendon Press, 2004).
- [37] E. G. Dalla Torre, E. Demler, and A. Polkovnikov, Universal rephasing dynamics after a quantum quench via sudden coupling of two initially independent condensates, *Phys. Rev. Lett.* **110**, 090404 (2013).
- [38] Y. Frenkel and T. Kontorova, in russian, *Zh. Eksp. Teor. Fiz.* **8**, 1 (1938).
- [39] B. Hu and B. Li, Quantum Frenkel-Kontorova Model, *Physica A* **288**, 81 (2000), arXiv: cond-mat/0106424.
- [40] D. X. Horváth, I. Lovas, M. Kormos, G. Takács, and G. Zaránd, Nonequilibrium time evolution and rephasing in the quantum sine-gordon model, *Phys. Rev. A* **100**, 013613 (2019).
- [41] H. W. Broer, I. Hoveijn, M. v. Noort, C. Simó, and G. Vegter, The parametrically forced pendulum: A case study in 1 1/2 degree of freedom, *Journal of Dynamics and Differential Equations* **16**, 897 (2004).
- [42] S. Coleman, Quantum sine-gordon equation as the massive thirring model, *Phys. Rev. D* **11**, 2088 (1975).
- [43] Y. Suzumura, Collective modes and response functions for the bgd model, *Progress of Theoretical Physics* **61**, 1 (1979).
- [44] F. Cooper, P. Sodano, A. Trombettoni, and A. Chodos, O(n) symmetric extension of the sine-gordon equation, *Phys. Rev. D* **68**, 045011 (2003).
- [45] Y. D. Van Nieuwkerk and F. H. L. Essler, Self-consistent time-dependent harmonic approximation for the sine-Gordon model out of equilibrium, *Journal of Statistical Mechanics: Theory and Experiment* **2019**, 084012 (2019), publisher: IOP Publishing.
- [46] Y. D. Van Nieuwkerk and F. Essler, On the low-energy description for tunnel-coupled one-dimensional Bose gases, *SciPost Physics* **9**, 025 (2020), arXiv: 2003.07873.
- [47] M. Abramowitz and I. Stegun, eds., *Handbook of mathematical functions* (Dover, New York, 1972).
- [48] L. D. Landau and E. M. Lifshitz, *Quantum Mechanics : non-relativistic theory* (perg, New York, 1962).